8521 words from “Main Text” to the end (including list of TO coordinators and affiliations)

Final revision to submit by FEB 5th

Title: Environmental characteristics of Agulhas rings affect inter-ocean plankton transport

Authors: Emilie Villar[1]*, Gregory Farrant[2,3¶], Michael Follows[11¶], Laurence Garczarek[2,3¶], Sabrina Speich[5,22¶], Stéphane Audic[2,3], Lucie Bittner[2,3,4 †], Bruno Blanke[5], Jennifer R. Brum[6], Christophe Brunet[7], Raffaela Casotti[7], Alison Chase[8], John R. Dolan[9,10], Fabrizio d'Ortenzio[9,10], Jean-Pierre Gattuso[9,10], Nicolas Grima[5], Lionel Guidi[9,10], Christopher N. Hill[11], Oliver Jahn[11], Jean-Louis Jamet[12], Hervé Le Goff[13], Cyrille Lepoivre[1], Shruti Malviya[4], Eric Pelletier[14,15,16], Jean-Baptiste Romagnan[9,10], Simon Roux[6], Sébastien Santini[1], Eleonora Scalco[7], Sarah M. Schwenck[6], Atsuko Tanaka[4‡], Pierre Testor[13], Thomas Vannier[14,15,16], Flora Vincent[4], Adriana Zingone[7], Céline Dimier[2,3,4], Marc Picheral[9,10], Sarah Searson[9,10††], Stefanie Kandels-Lewis[17,18], *Tara* Oceans coordinators[§], Silvia G. Acinas[19], Peer Bork[17], Emmanuel Boss[8], Colomban de Vargas[2,3], Gabriel Gorsky[9,10], Hiroyuki Ogata[1‡‡], Stéphane Pesant[20,21], Matthew B. Sullivan[6], Shinichi Sunagawa[17], Patrick Wincker[14,15,16], Eric Karsenti[4,18]*, Chris Bowler[4]*, Fabrice Not[2,3¶¶]*, Pascal Hingamp[1¶¶]*, Daniele Iudicone[7¶¶]*

Affiliations:

[1]Aix Marseille Université, CNRS, IGS UMR 7256, 13288, Marseille, France.
[2]CNRS, UMR 7144, Station Biologique de Roscoff, Place Georges Teissier, 29680 Roscoff, France.
[3]Sorbonne Universités, UPMC Univ Paris 06, UMR 7144, Station Biologique de Roscoff, Place Georges Teissier, 29680 Roscoff, France.
[4]Ecole Normale Supérieure, Institut de Biologie de l’ENS (IBENS), and Inserm U1024, and CNRS UMR 8197, Paris, F-75005 France.
[5]Laboratoire de Physique des Océans (LPO) UMR 6523 CNRS-Ifremer-IRD-UBO, Brest, France.
[6]Department of Ecology and Evolutionary Biology, University of Arizona, Tucson, AZ, 85721, USA.
[7]Zoologica Anton Dohrn, Villa Comunale, 80121, Naples, Italy.
[8]School of Marine Sciences, University of Maine, Orono, Maine, USA.
[9]Sorbonne Universités, UPMC Univ Paris 06, Observatoire Océanologique, F-06230 Villefranche-sur-mer, France.
[10]CNRS, UMR 7093, LOV, Observatoire Océanologique, F-06230 Villefranche-sur-mer, France.
[11]Department of Earth, Atmospheric and Planetary Sciences, Massachusetts Institute of Technology, Cambridge, USA.
[12]Université de Toulon, Laboratoire PROTEE-EBMA E.A. 3819, BP 20132, 83957 La Garde cedex, France.
[13]CNRS, UMR 7159, Laboratoire d'Oceanographie et du Climat LOCEAN, 4 place Jussieu, 75005, Paris, France.
[14]CEA - Institut de Génomique, GENOSCOPE, 2 rue Gaston Crémieux, 91057 Evry France.
[15]CNRS, UMR 8030, CP5706, Evry France.
[16]Université d'Evry, UMR 8030, CP5706, Evry France.
[17]Structural and Computational Biology, European Molecular Biology Laboratory, Meyerhofstr. 1, 69117 Heidelberg, Germany.
[18]Directors’ Research European Molecular Biology Laboratory Meyerhofstr. 1, 69117 Heidelberg, Germany.
[19]Department of Marine Biology and Oceanography Institute of Marine Science (ICM)-CSIC Pg. Marítim de la Barceloneta 37-49 Barcelona E08003 Spain.
[20]PANGAEA, Data Publisher for Earth and Environmental Science, University of Bremen, Bremen, Germany.
[21]MARUM, Center for Marine Environmental Sciences, University of Bremen, Bremen, Germany.
[22]Department of Geosciences, Laboratoire de Météorologie Dynamique (LMD), Ecole Normale Supérieure, 24 rue Lhomond, 75231 Paris Cedex 05 France.
§ Tara Oceans coordinators are listed in the acknowledgments.

† Current address: CNRS FR3631, Institut de Biologie Paris-Seine, F-75005, Paris, France / Sorbonne Universités, UPMC Univ Paris 06, Institut de Biologie Paris-Seine (IBPS), F-75005, Paris, France.
‡ Current address: Muroran Marine Station, Field science center for northern biosphere, Hokkaido university, Japan.
†† Current address: CMORE, University Hawaii, Honolulu, USA.
‡‡ Current address: Institute for Chemical Research, Kyoto University, Gokasho, Uji, Kyoto, 611-001, Japan.
¶ These authors contributed equally to this work.
¶¶ These authors contributed equally to this work.
*Correspondence to: villar@igs.cnrs-mrs.fr, not@sb-roscoff.fr, hingamp@igs.cnrs-mrs.fr, iudicone@szn.it, karsenti@embl.de, cbowler@biologie.ens.fr.

Abstract: Agulhas rings provide the principal route for ocean waters to circulate from the Indo-Pacific to the Atlantic basin. Their influence on global ocean circulation is well known but but their role in plankton transport is unknown. We show that while the coarse taxonomic structure of plankton communities is continuous across the Agulhas choke point, South Atlantic plankton diversity is altered compared to Indian Ocean source populations. Modelling and *in situ* sampling of a young Agulhas ring indicate that strong vertical mixing drives complex nitrogen cycling, shaping community metabolism and biogeochemical signatures as the ring and associated plankton transit westwards. The peculiar local environment inside Agulhas rings may provide a selective mechanism contributing to the limited dispersal of Indian Ocean plankton populations into the Atlantic.

One Sentence Summary: Differences in plankton richness between the South Atlantic and Indian Oceans may be due to a selective environment inside Agulhas rings.

Main Text:

The Agulhas Current, which flows down the east coast of Africa, leaks from the Indo-Pacific Ocean into the Atlantic Ocean (1). This leakage, a choke point to heat and salt distribution across the world's oceans, has been increasing over the last decades (2). The influence of the Agulhas leakage on global oceanic circulation makes this area a sensitive lever in climate change scenarios (3). Agulhas leakage has been a gateway for planetary-scale water transport since the early Pleistocene (4), but diatom fossil records suggest it is not a barrier to plankton dispersal (5). Most of the Agulhas leakage occurs through huge anticyclonic eddies known as Agulhas Rings. These 100 to 400 km diameter rings bud from Indian Ocean subtropical waters at the Agulhas Retroflection (1). Each year, up to half a dozen Agulhas rings escape the Indian Ocean, enter Cape Basin and drift north-westerly across the South Atlantic, reaching the South American continent over the course of several years (1,6). During their transit, strong westerly "roaring forties" winds prevalent in the southern 40s and 50s latitudes cause intense cooling and mixing in Agulhas rings (7).

Here we studied the effect of Agulhas rings and the environmental changes they sustain on plankton dispersal. Plankton, such as microalgae which produce half of the atmospheric oxygen and are at the base of open ocean ecosystems, play an essential role in the functioning of the biosphere. Their dispersal is critical for marine ecosystem resilience in the face of environmental change (8). As part of the *Tara* Oceans expedition (9), we describe taxonomic and functional plankton assemblages inside Agulhas rings and across the three oceanic systems which converge at the Agulhas choke point: The western Indian Ocean subtropical gyre, the South Atlantic Ocean gyre, and the Southern Ocean below the Antarctic Circumpolar Current (Fig. 1).

Physical and biological oceanography of the sampling sites

The Indian, South Atlantic and Southern Ocean were each represented by three sampling sites visited between May 2010 and January 2011 (fig. 1 & table S1). A variety of environmental conditions were represented (10). We first sampled the two large contiguous Indian and South Atlantic subtropical gyres and the Agulhas ring structures that maintain the physical connection between them. On the western side of the Indian Ocean, station TARA_052 was characterized by tropical, oligotrophic conditions. Station TARA_064 was located within an anticyclonic eddy representing the Agulhas Current recirculation. Station TARA_065 was located at the inner edge of the Agulhas Current on the South African slope that feeds the Agulhas retroflection and Agulhas ring formation (3). In the South Atlantic Ocean, station TARA_070, sampled in late winter, was located in the eastern subtropical Atlantic basin. Station TARA_072 was located within the tropical circulation of the South Atlantic Ocean, Station TARA_076 was at the north-west extreme of the South Atlantic subtropical gyre. Two stations (TARA_068 & TARA_078) from the west and east South Atlantic Ocean sampled Agulhas rings. Three stations (TARA_082, TARA_084, TARA_085) in the Southern Ocean were selected to sample the Antarctic Circumpolar Current frontal system. Station TARA_082 sampled sub-Antarctic waters flowing northward along the Argentinian slope, waters that flow along the Antarctic Circumpolar Current (11) with characteristics typical of summer sub-Antarctic surface waters and are stratified by seasonal heating. Station TARA_084 was located on the southern part of the Antarctic Circumpolar Current, in the Drake Passage between the Polar Front and the South Antarctic Circumpolar Current front (11). Station TARA_085 was located on the southern edge of the South Antarctic Circumpolar Current front with waters typical of polar regions.

We compared overall plankton community structures between the three oceans using imaging and genetic surveys of samples from the epipelagic zone of each station (12). Prokaryote, phyto- and zooplankton assemblages were similar across Indian and South Atlantic Ocean samples, but different from Southern Ocean samples (Fig. 2A). In Indian and South Atlantic Ocean, zooplankton communities were dominated by Calanoida, Cyclopoida (Oithonidae) and Poecilostomatoida copepods (12); phytoplankton communities were mainly composed of chlorophytes, pelagophytes and haptophytes (12). In contrast, Southern Ocean zooplankton communities were distinguished by abundance of *Limacina* spp. gastropods and few Poecilostomatoida copepods. Southern Ocean phytoplankton were primarily diatoms and haptophytes. The divergence was even more conspicuous with respect to prokaryotes, in that cyanobacteria, dominant in Indian and South Atlantic Ocean, were absent in Southern Ocean. Southern Ocean had a high proportion of Flavobacteria and Rhodobacterales (12). Virus concentrations in the <0.2 μm size fractions were significantly lower in the southernmost Southern Ocean station (13). Viral particles were significantly smaller in two of the three Southern Ocean sampling sites and two Southern Ocean viromes had significantly lower richness compared to South Atlantic and Indian Ocean (13). Although nucleocytoplasmic large DNA viruses were similarly distributed in South Atlantic and Indian Ocean (12), two Southern Ocean sites contained coccolithoviruses also found in the TARA_068 Agulhas ring but not in the other Indian and South Atlantic stations.

Biological connection across the Agulhas choke point

Genetic material as represented by rDNA sequences showed exchange patterns across the oceans (shared barcode richness, 14). Despite a smaller interface between Indian and South Atlantic Oceans than either have with the Southern Ocean, over three times more genetic material was in common between Indian and South Atlantic Oceans than either had with the Southern Ocean (Fig. 2B, 15). Indeed, the Indian-South Atlantic inter-ocean shared barcodes richness (32±5%) was not significantly different from typical intra-ocean values (37±7%, Tukey post-hoc 0.95 confidence). Shared barcode richness involving the Southern Ocean was significantly lower (9±3%, Fig. 2C). We found that the proportion of whole shotgun metagenomic reads shared between samples, both intra-oceanic and Indian-South Atlantic inter-ocean similarities were in the 18-30% range, whereas inter-ocean similarities with Southern Ocean samples were only 5-6% (16). These results reveal a strong genetic connection between the Indian and Atlantic Oceans, despite the separation between their physical basins.

Nonetheless, differences on either side of the Agulhas choke point were evident. We found that prokaryote barcode richness was greater in the South Atlantic than in the Indian Ocean (Fig. 3A, 0.2-3 μm size fraction). The opposite trend characterized eukaryotes larger than 20 μm in size. We cannot rule out the possibility that the higher prokaryote diversity observed in South Atlantic Ocean might be due to a protocol artefact resulting from a difference in prefiltration pore size from 1.6 μm (Indian Ocean) to 3 μm (South Atlantic and Southern Ocean). As also evident from the pan-oceanic Tara Oceans dataset (17), smaller size fractions showed greater eukaryote diversity across the Agulhas system. In all size fractions we analyzed, samples from the Southern Ocean were less diverse than samples from the South Atlantic Ocean and Indian Ocean (Fig. 3A). When rDNA barcodes were clustered by sequence similarity and considered at operational taxonomic unit (OTU) level (14), over half (57%) of the OTUs contained higher sub-OTU barcode richness in Indian than in South Atlantic Ocean, whereas less than a third (32%) of OTUs were richer in South Atlantic Ocean, leaving only 11% as strictly cosmopolitan (Fig. 3B). Taken together, these 1307 OTUs represented 98% of the barcode abundance, indicating that the observed higher barcode richness within OTUs in the Indian Ocean was not conferred by the rare biosphere. Certain taxa displayed unusual sub-OTU richness profiles across the choke point. Consistent with their relatively large size, Opisthokonta (mostly copepods), Rhizaria (such as radiolarians) and Stramenopiles (in particular diatoms) had much higher sub-OTU barcode richness in the Indian Ocean, whereas only small sized Hacrobia (mostly haptophytes) showed modest increased sub-OTU barcode richness in the South Atlantic Ocean. The plankton filtering we observed in fractions above 20 μm through the Agulhas choke point might explain the reduction of marine nekton diversity from the Indian Ocean to the South Atlantic Ocean (18), by propagating up the food-web (19).

In situ sampling of two Agulhas rings

To understand whether the environment of Agulhas rings, the main transporters of water across the choke point, might act as a biological filter between Indian Ocean and South Atlantic Ocean, we analyzed data collected in both a young and an old Agulhas ring. The young ring sampled at station TARA_068 was located in Cape Basin west of South Africa, where rings are often observed after their formation at the Agulhas Retroflection (7,20). It was a large Agulhas ring that detached from the retroflection about 9-10 months prior to sampling. This ring first moved northward and then westward in the Cape Basin while interacting with other structures (red track in fig. 1b, 21). Ocean color data collected by satellite showed that surface chlorophyll concentrations were higher in the Cape Basin than at the retroflection, suggesting that deep

vertical mixing might have occurred in the Cape Basin (22). At the time of sampling, the anticyclonic Agulhas ring was 130-150 km in diameter, was about 30 cm higher than average sea surface, and was flanked by a 130-150 km cyclonic eddy to the north and a larger (> 200km) one to the east (Fig. 4A, 23). Thermosalinograph data showed that filaments of colder, fresher water surrounded the young ring core (Fig. 4A, 23). In order to position the biological sampling station close to the ring core, a series of Conductivity-Temperature-Depth casts (CTD) was performed (23, 24). The young Agulhas ring had a surface temperature and salinity of 16.8°C and 35.7 psu, respectively; and the isopycnal sloping could be traced down to CTD maximal depth (900-1000m). The core of the ring water was 5°C cooler than Indian Ocean subtropical source waters at similar latitudes (TARA_065, table S1), typical for the subtropical waters south of Africa (17.8°C, 35.56 psu, respectively, 25). The mixed layer of the young ring was deep (>250m) compared to seasonal cycles of the mixed layer depths in the region (50-100m, fig. 4C), typical of Agulhas rings (26). At larger scales (Fig. 4B, 24), steep spatial gradients were observed, with fresher and colder water in the Cape Basin than in the Agulhas Current because of both lateral mixing with waters from the South and surface fluxes. This confirms that the low temperature of the young Agulhas ring is a general feature of this Indian to South Atlantic Ocean transitional basin. Air-sea exchanges of heat and momentum promoted convection in the ring core, which was not compensated by lateral mixing and advection. The core of the Agulhas ring thus behaved as a sub-polar environment traveling across sub-tropical regions.

At station TARA_078 we sampled a second structure whose origins were in the Agulhas Retroflection, likely a 3-year-old Agulhas ring. This old ring, having crossed the South Atlantic Ocean, was being absorbed by the western boundary current of the South Atlantic subtropical gyre. The structure sampled at station TARA_078 was characterized by a warm salty core (27). As for the young Agulhas ring sampled, the old ring also had a 100m deeper pycnocline than surrounding waters, typical of large anticyclonic structures.

The plankton assemblage of both Agulhas rings most closely resembled the assemblages found in Indian and South Atlantic samples (Fig. 2A). At higher resolution, barcodes (Fig. 2B & 2C) and metagenomic reads (16) shared between the Agulhas rings and the Indian or South Atlantic samples showed that the young ring was genetically distinct from both Indian and South Atlantic samples, whereas the old ring was similar to its surrounding South Atlantic samples (Tukey post-hoc .95 confidence). Light microscopy analyses revealed some plankton groups specific to the young Agulhas ring, such as *Pseudo-nitzschia* spp. which represented 20% of the phytoplankton counts but less than 10% in all other stations (12). Other potentially circumstantial plankton characteristic of the young Agulhas ring included the tintinnid *Dictyocysta pacifica* (12), the diatom *Corethron pennatum* (12), and the dinoflagellate *Tripos limulus* (12). A tiny (less than 15 µm long) pennate diatom from the genus *Nanoneis,* which we saw only in the young Agulhas ring and Indian Ocean stations around the African coasts (28), was an example of the Indo-Atlantic plankton diversity filtering observed at rDNA barcode level and corroborated by microscopy. OTU clustered barcodes revealed a variety of young Agulhas ring sub-OTU richness patterns compared to source and destination oceans (Fig. 5A). Amongst Copepoda, *Gaetanus variabilis* and *Corycaeus speciosus* were the more cosmopolitan species (Fig. 5B), whilst *Bradya* species found in the young ring were mainly similar to those from the Indian Ocean. *Acartia negligens* and *Neocalanus robustior* displayed high levels of barcode richness specific to each side of the Agulhas choke point. Bacillariophyceae were heavily filtered from Indian to South Atlantic Oceans (Fig. 5C), and most OTUs (17 out of 20) were absent in the young ring, suggesting diversity filtering could take place earlier in the ring's nine months

history. Consistent with the observed particularities of the plankton in the young ring, continuous underway optical measurements showed that the ring core photosynthetic community differed significantly from surrounding waters (29-31). Intermediate size cells, and relatively low content of photo-protective pigments, reflected low growth irradiance and suggested a transitional physiological state. Thus, the plankton community in the young Agulhas ring had diverged from plankton communities typical of its original Indian waters, but, even nine months after formation, had not converged with its surrounding South Atlantic waters.

Deep mixing in Agulhas rings promotes plankton bloom

The upper water column of the young ring showed a high nitrite concentration (>0.5 mmol.m-3) (Fig. 4D, 32). This observation, along with its particularly deep mixed layer (>250m), suggested that as Agulhas rings proceed westward in the Cape Basin, vigorous deep mixing of their weakly stratified waters may have entrained nitrate and stimulated phytoplankton blooms. Typically, fresh organic material would then either be exported as sinking particles or locally recycled, sustaining heterotrophic production of ammonium which would, in turn, be consumed by photoautotrophs in the euphotic layer but nitrified below. The resulting nitrite, eventually oxidized to nitrate, might remain evident at subsurface as observed in the nitrite anomaly of the young ring explored here. This hypothesis was supported by numerical simulations of the Massachusetts Institute of Technology general circulation model (33) which resolved Agulhas rings, their phytoplankton populations and associated nutrient cycling (Fig. 6A). We tracked 12 Agulhas rings in the ocean model and characterized their near-surface biogeochemical cycles (Fig. 6B, 34). As the rings moved westwards, storms enhanced surface heat loss stimulating convection and the entrainment of nitrate. In the model simulations, proliferation of phytoplankton generated subsurface nitrite, which persisted because phytoplankton were light limited at depth and because nitrification was suppressed by light at the surface (35). The associated blooms were dominated by large opportunistic phytoplankton and nitrate-metabolizing *Synechococcus* spp. analogs, whereas populations of *Prochlorococcus* spp. analogs dominated the quiescent periods (34). Each of the 12 simulated Agulhas rings exhibited this pattern in response to surface forcing by weather systems, and all rings maintained a persistent subsurface nitrite maximum in the region, as observed in TARA_068 and in other biogeochemical surveys (36).

The nitrite peak observed at TARA_068 in the young Agulhas ring was associated with a differential representation of nitrogen metabolism genes between the ring and the surrounding South Atlantic and Indian Oceans metagenomes derived from 0.2-3 μm size fractions (Fig. 7, 37). Agulhas ring over-represented KEGG (Kyoto Encyclopedia of Genes and Genomes, 61) orthologs (KOs) were involved in both nitrification and denitrification, likely representing the overlap between plankton assemblages involved in the conversion of nitrate to nitrite on the one hand, and in denitrification of the accumulating nitrite on the other. Distinct KOs involved in successive denitrification steps were found to be encoded by similar plankton taxa. For instance KO10945 and KO10946 involved in ammonium nitrification and KO00368 subsequently involved in nitrite to nitrous oxide denitrification appeared mostly encoded by Nitrosopumilaceae archaea. KO00264 and KO01674 involved in ammonium assimilation were mostly assigned to eukaryotic Mamiellales, whilst the opposite KO00367 and KO00366 involved in dissimilatory nitrite reduction to ammonium followed by KO01725 involved in ammonium assimilation were encoded by picocyanobacteria. In the specific case of the picocyanobacteria, metagenomic reads corresponding to *nirA* genes showed that the observed young Agulhas ring

KO00366 (dissimilatory nitrite reduction) enrichment was mainly due to the over-representation of genes from *Prochlorococcus* (Fig. 8B). This enrichment was found to be associated with a concomitant shift in population structure from *Prochlorococcus* High Light II ecotypes (HLII mostly lacking *nirA* genes) to co-dominance of High Light I (HLI) and Low Light I (LLI) ecotypes. Indeed, among the several *Prochlorococcus* and *Synechococcus* ecotypes identified based on their genetic diversity and physiology (38,39), neutral marker (*petB*, fig. 8A) recruitments showed that dominant clades in the Indian Ocean upper mixed layer were *Prochlorococcus* HLII and *Synechococcus* clade II, as expected given the known (sub)tropical preferenda of these groups (40). Both clades nearly completely disappeared (less than 5%) in the mixed cold waters of the young ring and only began to increase again when the surface water warmed up along the South Atlantic Ocean transect. Conversely, young ring water was characterized by a large proportion of *Prochlorococcus* HLI and LLI and *Synechococcus* clade IV, two clades typical of temperate waters. Besides temperature, the *Prochlorococcus* community shift from HLII to HLI + LLI observed in the young ring was likely also driven by the nitrite anomaly. Indeed, while most *Synechococcus* strains isolated so far are able to use nitrate, nitrite and ammonium, only the *Prochlorococcus* LLI and IV and some populations of HL clades, having acquired the *nirA* gene by lateral gene transfer, are able to assimilate nitrite. In the young ring, over-representation of cyanobacterial orthologs involved in nitrite reduction could thus have resulted from environmental pressure selecting LLI (87% of the nirA recruitments) and HLI populations (13%) that possessed this ability. Since the capacity to assimilate nitrite in this latter ecotype reflects the availability of this nutrient in the environment (41), these *in situ* observations of picocyanobacteria indicated that the nitrogen cycle disturbance occurring in the young ring exerts community wide selective pressure on Agulhas ring plankton.

Discussion

We found that whether or not the Agulhas choke point is considered a barrier to plankton dispersal depends on the taxonomic resolution at which the analysis is performed. At coarse taxonomic resolution, our observations of Indo-Atlantic continuous plankton structure - from viruses to fish larvae - suggested unlimited dispersal, consistent with previous reports (5, 42). However, at finer resolution our genetic data revealed that the Agulhas choke point strongly affects patterns of plankton genetic diversity. As anticipated in (5), the diversity filtering by Agulhas Rings likely escaped detection using fossil records because of the limited taxonomic resolution afforded by fossil diatom morphology (42). The community wide evidence presented here confirm observations on individual living species (43,44), suggesting that dispersal filters mitigate the panmictic ocean hypothesis for plankton above 20 µm.

The lower diversity we observed in South Atlantic Ocean for micro- and mesoplankton (>20 µm) may be due to local abiotic/biotic pressure or to limitations in dispersal (33, 45). Although biogeography emerging from a model with only neutral drift (46) predicts basin-to-basin genetic differences that are qualitatively consistent with our data, the observed acquisition of *nirA* genes by HLI *Prochlorococcus* in the young Agulhas ring indicates selection is at work in Agulhas rings. Based on our analysis of two Agulhas rings, we propose that environmental disturbances in Agulhas rings reshape their plankton diversity as they travel from Indian Ocean to South Atlantic Ocean. As a result, South Atlantic Ocean plankton diversity differs from that of the Indo-Pacific basin despite being directly downstream. Thus, environmental selection applied at a choke point in ocean circulation constitutes a barrier to dispersal. Furthermore, we show that taxonomic groups were not equally affected by the ring transport, both within and between phyla,

with a noticeable effect of organism size. The differential effects due to organism size highlight the difficulty in generalizing ecological and evolutionary rules from limited sampling of species or functional types. .

Considering sensitivity of Agulhas leakage to climate change (1, 49), better understanding of the plankton dynamics in Agulhas rings will be required if we are to understand and predict ecosystem resilience at the planetary scale. Considering the breadth of changes already observed in the 9-month-old Agulhas ring, it would be interesting to acquire samples from specific Agulhas rings tracked from early formation to dissipation. Finally, our data suggest that the abundance of Indian Ocean species in South Atlantic Ocean sedimentary records, used as proxies of Agulhas Leakage intensity (4), may actually also depend on the intensity of the Agulhas ring physical disturbances.

Materials & Methods

Sampling

The Tara Oceans sampling protocols schematized in Karsenti et al. (11) are described in Pesant et al. (50), specific methods for 0.8-5, 20-180 & 180-2000 µm size fractions in de Vargas et al. (17), for 0.2-3 µm size fractions in Sunagawa et al. (51), and for the <0.2 µm size fraction in Brum et al. (52). Due to their fragility, 1.6 µm glass fiber filters initially used for prokaryote sampling were replaced by more resistant 3 µm polycarbonate filters from station TARA_066 onwards. In the present text, both 0.2-1.6 µm and 0.2-3 µm prokaryote size fractions are simply referred to as 0.2-3 µm.

Data acquisition

A range of analytical methods covering different levels of taxonomic resolution (pigments, flow cytometry, optical microscopy, marker gene barcodes, metagenomics) were used to describe the planktonic composition at each sampled station. Viruses from the <0.2 µm size fraction were studied both by epifluorescence microscopy, quantitative transmission electron microscopy and by sequencing DNA as described in Brum *et al.* (52). Flow cytometry was used to discriminate high DNA content bacteria (HNA), low DNA content bacteria (LNA), Prochlorococcus and Synechococcus picocyanobacteria, as well as two different groups (based on their size) of photosynthetic picoeukaryotes as described previously (53). Pigment concentrations measured by High Performance Liquid Chromatography (HPLC) were used to estimate the dominant classes of phytoplankton using the CHEMTAX procedure (54). Tintinnids, diatoms and dinoflagellates were identified and counted by light microscopy from the 20-180 µm lugol or formaldehyde fixed size fraction. Zooplankton enumeration was performed on formol fixed samples using the ZOOSCAN semi-automated classification of digital images (55). Sequencing, clustering and annotation of 18S-V9 rDNA barcodes are described in de Vargas *et al.* (17). Metagenome sequencing, assembly and annotation are described in Sunagawa *et al.* (51). NCLDV taxonomic assignations in the 0.2-3 µm samples were carried out using 18 lineage specific markers as described in Hingamp *et al.* (56). Virome sequencing and annotation are described in Brum *et al.* (46).

Data analysis

Origin of sampled Agulhas rings

Using visual and automated approaches, the origins of the TARA_068 and TARA_078 stations was traced back from the altimetric daily data (Fig. 1, 21). The automated approach used either

the Lagrangian tracing of numerical particles initialized in the centre of a given structure and transported by the geostrophic velocity field calculated from sea surface height gradients, or the connection in space and time of adjacent extreme values in sea level anomaly maps.

V9 rDNA barcodes

To normalize for differences in sequencing effort, V9 rDNA barcode libraries were resampled 50 times for the number of reads corresponding to the smallest library in each size fraction: 0.8-5 µm: 776,358 reads, 20-180 µm: 1,170,592 reads and 180-2000 µm: 767,940 reads. V9 rDNA barcode counts were then converted to the average number of times seen in the 50 resampling events and barcodes with less than 10 reads were removed as potential sequencing artefacts. We used down-sampled barcode richness (number of distinct V9 rDNA barcodes) as a diversity descriptor since considering V9 rDNA barcode abundances to compare plankton assemblages would likely be biased due: i/ to technical limitations described in de Vargas et al. (17), and ii/ to seasonality effects induced by the timing of samplings (Table S1). Barcode richness was well correlated with Shannon and Simpson indexes (0.94 and 0.78, respectively). The shared barcode richness between each pair of samples (14) was estimated by counting for the three larger size fractions (0.8-5, 20-180 & 180-2000 µm) the proportion of V9 rDNA barcodes 100% identical over their whole length. V9 rDNA barcodes were clustered into OTUs by SWARM clustering as described by de Vargas et al. (17). The sub-OTU richness comparison between two samples s1 and s2 (14) produces three values: the number of V9 rDNA barcodes in common, the number of V9 rDNA barcodes unique to s1, and the number of V9 rDNA barcodes unique to s2. These numbers can be represented directly as bar graphs (Fig. 3B) or as dot plots of specific V9 rDNA barcode richness (Fig. 5).

Metagenomic analysis

Similarity was estimated using whole shotgun metagenomes for all four available size fractions (0.2-3, 0.8-5, 20-180 & 180-2 000 µm). Because pairwise comparisons of all raw metagenome reads is intractable given the present data volume, we used a heuristic where two metagenomic 100 bp reads were considered similar if at least two non overlapping 33 bp kmers were strictly identical (Compareads method, 60). For prokaryotic fractions (0.2-3 µm), taxonomic abundance was estimated using the number of 16S miTags (51). The functional annotation, taxonomic assignation and gene abundance estimation of the pan oceanic Ocean Microbial Reference Gene Catalog (OMRGC, 243 samples including all those analysed here) generated from Tara Oceans 0.2-3 µm metagenomic reads are described in Sunagawa *et al.* (51). Gene abundances were computed for the set of genes annotated to nitrogen metabolism KEGG ortholog (KO, 61) group by counting the number of reads from each sample that mapped to each KO associated gene. Abundances were normalized as Reads Per Kilobase per Million mapped reads (RPKM). Gene abundances were then aggregated (summed) for each KO group. To compare abundances between the young ring (TARA_068) and other stations, a t-test was used. KOs with a p-value < 0.05 and a total abundance (over all stations) > 10 were considered as significant (37). Prochlorococcus and Synechococcus community composition was analyzed in the 0.2-3 µm size fraction at the clade level by recruiting reads targeting the high resolution marker gene petB, coding for cytochrome b6 (62). The petB reads were first extracted from metagenomes using BLASTx+ against the petB sequences of Synechococcus sp. WH8102 and Prochlorococcus marinus MED4. These reads were subsequently aligned against a reference dataset of 270 petB sequences using BLASTn (with parameters set at -G 8 -E 6 -r 5 -q -4 -W 8 -e 1 -F "m L" -U T). petB reads exhibiting $> 80\%$ identity over $> 90\%$ of sequence length were then taxonomically assigned to the clade of the best BLAST hit. Read counts per clade were normalized based on the

sequencing effort for each metagenomic sample. A similar approach was used with nirA (KO 00366) and narB genes (KO 00367) which were highlighted in the nitrogen-related KO analysis (Fig. 8). Phylogenetic assignment was realized at the highest possible taxonomic level using a reference dataset constituted of sequences retrieved from Cyanorak v2 (www.sbroscoff. fr/cyanorak/) and GOS (63, 41) databases.

Nitrogen cycle modelling

Numerical simulations of global ocean circulation were based on the Massachusetts Institute of Technology general circulation model (MITgcm; 64) incorporating biogeochemical and ecological components (65,66). It resolved mesoscale features in the tropics and was eddy permitting in sub-polar regions. The physical configurations were integrated from 1992 to 1999 and constrained to be consistent with observed hydrography and altimetry (67). Three inorganic fixed nitrogen pools were resolved: nitrate, nitrite and ammonium, as well as particulate and dissolved detrital organic nitrogen. Phytoplankton types were able to use some or all of the fixed nitrogen pools. Aerobic respiration and remineralization by heterotrophic microbes was parameterized as a simple sequence of transformations from detrital organic nitrogen, to ammonium, then nitrification to nitrite and nitrate. In accordance with empirical evidence (35), nitrification was assumed to be inhibited by light. Nitrification is described in the model by simple first order kinetics, with rates tuned to qualitatively capture the patterns of nitrogen species in the Atlantic (66).

Continuous spectral analysis

A continuous flow-through system equipped with a high-spectral-resolution spectrophotometer (AC-S, WET Labs, Inc.) was used for data collection during the Tara Oceans expedition as described previously (68). Phytoplankton pigment concentrations, estimates of phytoplankton size γ, total chlorophyll a concentration, and particulate organic carbon (POC) are derived from the absorption and attenuation spectra (69) for the 1-km2-binned *Tara* Oceans data set available at PANGAEA under project label “Tara Oceans” (http://www.pangaea.de).

References and Notes:

1. Biastoch, C. W. Böning, J. R. E. Lutjeharms, Agulhas leakage dynamics affects decadal variability in Atlantic overturning circulation, Nature 4489–(2008).
2. Biastoch, C. W. Böning, F. U. Schwarzkopf, J. R. E. Lutjeharms, Increase in Agulhas leakage due to poleward shift of Southern Hemisphere westerlies, Nature 4495–(2009).
3. L. M. Beal, W. P. M. D. Ruijter, A. Biastoch, R. Zahn, S. W. G. 1On the role of the Agulhas system in ocean circulation and climate, Nature 4429–(2011).
4. F. J. C. Peeters et al., Vigorous exchange between the Indian and Atlantic oceans at the end of the past five glacial periods, Nature 4661–(2004).
5. P. Cermeño, P. G. Falkowski, Controls on Diatom Biogeography in the Ocean, Science 31539–1(2009).
6. A. L. Gordon, Oceanography: The brawniest retroflection. Nature. 4904–(2003).
7. H. M. van Aken et al., Observations of a young Agulhas ring, Astrid, during MARE in March 20Deep Sea Research Part II: Topical Studies in Oceanography. 167–(2003).
8. J. R. Bernhardt, H. M. Leslie, Resilience to Climate Change in Coastal Marine Ecosystems, Annual Review of Marine Science, 371-(2013).
9. E. Karsenti *et al.*, A Holistic Approach to Marine Eco-Systems Biology, PLoS Biol e1001(2011).
10. Companion web site tables W2-W3 available at http://www.igs.cnrs-mrs.fr/Tara_Agulhas/#TablesW
11. A.H. Orsi, T. Whitworth III, W. D. Nowlin Jr., On the meridional extent and fronts of the Antarctic Circumpolar Current. Deep-Sea Res. Part 1 641–(1995)
12. Companion web site tables W4-W12 available at http://www.igs.cnrs-mrs.fr/Tara_Agulhas/#TablesW
13. Companion web site figure W1 available at http://www.igs.cnrs-mrs.fr/Tara_Agulhas/#FigW1
14. Companion web site figure W2 available at http://www.igs.cnrs-mrs.fr/Tara_Agulhas/#FigW2
15. Companion web site tables W13-W14 available at http://www.igs.cnrs-mrs.fr/Tara_Agulhas/#TablesW

16. Companion web site figure W3 available at http://www.igs.cnrs-mrs.fr/Tara_Agulhas/#FigW3
17. de Vargas *et al.*, Eukaryotic plankton diversity in photic global ocean, submitted.
18. W. Bowen, L. A. Rocha, R. J. Toonen, S. A. Karl, The origins of tropical marine biodiversity, Trends in Ecology & Evolution 359–(2013).
19. R. L. Cunha et al., Ancient Divergence in the Trans-Oceanic Deep-Sea Shark Centroscymnus crepidater. PLoS ONE. e49(2012).
20. Schmid et al., Early evolution of an Agulhas Ring. Deep Sea Research Part II: Topical Studies in Oceanography. 141–(2003).
21. Companion web site figure W4 available at http://www.igs.cnrs-mrs.fr/Tara_Agulhas/#FigW4
22. Companion web site figure W5 available at http://www.igs.cnrs-mrs.fr/Tara_Agulhas/#FigW5
23. Companion web site figure W6 available at http://www.igs.cnrs-mrs.fr/Tara_Agulhas/#FigW6
24. Companion web site figure W7 available at http://www.igs.cnrs-mrs.fr/Tara_Agulhas/#FigW7
25. L. Gordon, J. R. Lutjeharms, M. L. Gründlingh, Stratification and circulation at the Agulhas Retroflection. Deep Sea Research Part A. Oceanographic Research Papers. 565–(1987).
26. V. Faure, M. Arhan, S. Speich, S. Gladyshev, Heat budget of the surface mixed layer south of Africa. Ocean Dynamics. 1441–1(2011).
27. Companion web site figure W8 available at http://www.igs.cnrs-mrs.fr/Tara_Agulhas/#FigW8
28. Companion web site figure W9 available at http://www.igs.cnrs-mrs.fr/Tara_Agulhas/#FigW9
29. Companion web site text W1 available at http://www.igs.cnrs-mrs.fr/Tara_Agulhas/#TextW1
30. Companion web site figure W10 available at http://www.igs.cnrs-mrs.fr/Tara_Agulhas/#FigW10
31. Companion web site figure W11 available at http://www.igs.cnrs-mrs.fr/Tara_Agulhas/#FigW11
32. Companion web site figure W12 available at http://www.igs.cnrs-mrs.fr/Tara_Agulhas/#FigW12
33. S. Clayton, S. Dutkiewicz, O. Jahn, M. J. Follows, Dispersal, eddies, and the diversity of marine phytoplankton, Limnology & Oceanography: Fluids & Environments 182–(2013).
34. Companion web site figure W13 available at http://www.igs.cnrs-mrs.fr/Tara_Agulhas/#FigW13
35. R. J. Olson, Differential photoinhibition of marine nitrifying bacteria: a possible mechanism for the formation of the primary nitrite maximum. J. mar. Res. 227–(1981).
36. S. Levitus et al., The World Ocean Database. Data Science Journal. WDS229–WDS(2013).
37. Companion web site table W15 available at http://www.igs.cnrs-mrs.fr/Tara_Agulhas/#TablesW
38. D. J. Scanlan *et al.*, Ecological genomics of marine picocyanobacteria. Microbiology and Molecular Biology Reviews. 249–(2009).
39. Z. I. Johnson *et al.*, Niche Partitioning Among Prochlorococcus Ecotypes Along Ocean- Scale Environmental Gradients. Science. 31737–1(2006).
40. K. Zwirglmaier *et al.*, Global phylogeography of marine Synechococcus and Prochlorococcus reveals a distinct partitioning of lineages among oceanic biomes. Environmental microbiology. 147–(2008).
41 A. C. Martiny, S. Kathuria, P. M. Berube, Widespread metabolic potential for nitrite and nitrate assimilation among Prochlorococcus ecotypes. PNAS. 110787–10(2009).
42. Hubert *et al.*, A Constant Flux of Diverse Thermophilic Bacteria into the Cold Arctic Seabed. Science. 31541–1(2009).
43 K. C. Churchill, Á. Valdés, D. Ó. Foighil, Afro-Eurasia and the Americas present barriers to gene flow for the cosmopolitan neustonic nudibranch Glaucus atlanticus. Mar Biol. 18(2014).
44. N. Selje, M. Simon, T. Brinkhoff, A newly discovered Roseobacter cluster in temperate and polar oceans. Nature. 4445–(2004).
45. Casteleyn *et al.*, Limits to gene flow in a cosmopolitan marine planktonic diatom. PNAS. 112952–12(2010).
46. L. Hellweger, E. van Sebille, N. D. Fredrick, Biogeographic patterns in ocean microbes emerge in a neutral agent-based model. Science. 31346–1(2014).
47. D. H. Janzen, Why mountain passes are higher in the tropics. American Naturalist 233-(1967).
48. G. Wang, M. E. Dillon, Recent geographic convergence in diurnal and annual temperature cycling flattens global thermal profiles. Nature Climate Change 988–9(2014).
49 C. Backeberg, P. Penven, M. Rouault, Impact of intensified Indian Ocean winds on mesoscale variability in the Agulhas system, Nature Clim. Change 608–(2012).
50. S. Pesant *et al.*, Tara Oceans Data: A sampling strategy and methodology for the study of marine plankton in their environmental context. Intended for publication at NPG Scientific Data (in review), in synchrony with Science publications.
51 S. Sunagawa *et al.*, Structure and function of the global ocean microbiome, submitted.
52. J. R. Brum *et al.*, Global patterns and ecological drivers of ocean viral communities, submitted.

53 J. M. Gasol, P. A. Del Giorgio, Using flow cytometry for counting natural planktonic bacteria and understanding the structure of planktonic bacterial communities; Scientia Marina. 64 (2000).
54. M. Mackey, D. Mackey, H. Higgins, S. Wright, CHEMTAX - a program for estimating class abundances from chemical markers: application to HPLC measurements of phytoplankton. Mar. Ecol. Progr. Ser. 1265–(1996).
55 G. Gorsky *et al.*, Digital zooplankton image analysis using the ZooScan integrated system. J. Plankton Res. 285–(2010).
56. P. Hingamp *et al.*, Exploring nucleo-cytoplasmic large DNA viruses in Tara Oceans microbial metagenomes. ISME J. 7, 1678–1(2013).
57. Tara Oceans Consortium, Coordinators; Tara Oceans Expedition, Participants (2014): Registry of selected samples from the Tara Oceans Expedition (2009-2013). doi:10.1594/PANGAEA.840721 http://doi.pangaea.de/10.1594/PANGAEA.840721
58. Chaffron, Samuel; Guidi, Lionel; D'Ovidio, Francesco; Speich, Sabrina; Audic, Stephane; De Monte, Silvia; Iudicone, Daniele; Picheral, Marc; Pesant, Stephane; Tara Oceans Consortium, Coordinators; Tara Oceans Expedition, Participants (2014): Contextual environmental data of selected samples from the Tara Oceans Expedition (2009-2013). doi:10.1594/PANGAEA.840718 http://doi.pangaea.de/10.1594/PANGAEA.840718
59. Chaffron, Samuel; D'Ovidio, Francesco; Sunagawa, Shinichi; Acinas, Silvia G; Coelho, Luis Pedro; De Monte, Silvia; Salazar, Guilhem; Pesant, Stephane; Tara Oceans Consortium, Coordinators; Tara Oceans Expedition, Participants (2014): Contextual biodiversity data of selected samples from the Tara Oceans Expedition (2009-2013). doi:10.1594/PANGAEA.840698 http://doi.pangaea.de/10.1594/PANGAEA.840698
60. N. Maillet, C. Lemaitre, R. Chikhi, D. Lavenier, P. Peterlongo, Compareads: comparing huge metagenomic experiments. BMC Bioinformatics. S10 (2012).
61 M. Kanehisa et al., KEGG for linking genomes to life and the environment. Nucleic Acids Research. D(2008).
62. S. Mazard, M. Ostrowski, F. Partensky, D. J. Scanlan, Multi-locus sequence analysis, taxonomic resolution and biogeography of marine Synechococcus. Environmental Microbiology. 372–(2012).
63 B. Rusch *et al.*, The Sorcerer II Global Ocean Sampling Expedition: Northwest Atlantic through Eastern Tropical Pacific. PLoS Biol. 5, e77 (2007).
64. J. Marshall, A. Adcroft, C. Hill, L. Perelman, C. Heisey, A finite-volume, incompressible Navier Stokes model for studies of the ocean on parallel computers. J. Geophys. Res.-Oceans. 15753–5(1997).
65. M. J. Follows, S. Dutkiewicz, S. Grant, S. W. Chisholm, Emergent Biogeography of Microbial Communities in a Model Ocean. Science. 31843–1(2007).
66. S. Dutkiewicz, M. J. Follows, J. G. Bragg, Modeling the coupling of ocean ecology and biogeochemistry. Global Biogeochem. Cycles. GB4(2009).
67. Menemenlis *et al.*, ECCO2: High resolution global ocean and sea ice data synthesis. Mercator Ocean Quarterly Newsletter. 13–21 (2008).
68. A. Chase *et al.*, Decomposition of in situ particulate absorption spectra. Methods in Oceanography. 7, 110–(2013).
69. E. Boss *et al.*, The characteristics of particulate absorption, scattering and attenuation coefficients in the surface ocean; Contribution of the Tara Oceans expedition. Methods in Oceanography. 7, 52–62 (2013).

Acknowledgments:
We thank the commitment of the following people and sponsors: CNRS (in particular Groupement de Recherche GDR3280), European Molecular Biology Laboratory (EMBL), Genoscope/CEA, VIB, Stazione Zoologica Anton Dohrn, UNIMIB, Fund for Scientific Research – Flanders, Rega Institute, KU Leuven, The French Ministry of Research, the French Government 'Investissements d'Avenir' programmes OCEANOMICS (ANR-11-BTBR-0008), FRANCE GENOMIQUE (ANR-10-INBS-09-08), MEMO LIFE (ANR-10-LABX-54), PSL* Research University (ANR-11-IDEX-0001-02), ANR (projects POSEIDON/ANR-09-BLAN-0348, PHYTBACK/ANR-2010-1709-01, PROMETHEUS/ANR-09-PCS-GENM-217, TARAGIRUS/ ANR-09-PCS-GENM-218), European Union FP7 (MicroB3/No.287589, IHMS/HEALTH-F4-2010-261376), ERC Advanced Grant Award to CB (Diatomite: 294823),

Gordon and Betty Moore Foundation grant (#3790) to MBS, Spanish Ministry of Science and Innovation grant CGL2011-26848/BOS MicroOcean PANGENOMICS to SGA, TANIT (CONES 2010-0036) from the Agència de Gestió d´Ajusts Universitaris i Reserca to SGA, JSPS KAKENHI Grant Number 26430184 to HO, NASA Ocean Biology and Biogeochemistry program (NNX11AQ14G and NNX09AU43G) to EB, The Italian Research for the Sea (Flagship Project RITMARE) to DI, FWO, BIO5, Biosphere 2 to MBS. We also thank the support and commitment of Agnès b. and Etienne Bourgois, the Veolia Environment Foundation, Region Bretagne, Lorient Agglomeration, World Courier, Illumina, the EDF Foundation, FRB, the Prince Albert II de Monaco Foundation, the Tara schooner and its captains and crew. We thank MERCATOR-CORIOLIS and ACRI-ST for providing daily satellite data during the expedition. We are also grateful to the French Ministry of Foreign Affairs for supporting the expedition and to the countries who graciously granted sampling permissions. Tara Oceans would not exist without continuous support from 23 institutes (http://oceans.taraexpeditions.org). We also acknowledge excellent assistance from the European Bioinformatics Institute (EBI), in particular Guy Cochrane and Petra ten Hoopen, as well as the EMBL Advanced Light Microscopy Facility (ALMF), in particular Rainer Pepperkok. We thank Y. Timsit for stimulating scientific discussions and critical help during writing of the manuscript. The altimeter products were produced by Ssalto/Duacs and CLS with support from CNES. The authors further declare that all data reported herein are fully and freely available from the date of publication, with no restrictions, and that all of the samples, analyses, publications, and ownership of data are free from legal entanglement or restriction of any sort by the various nations whose waters the Tara Oceans expedition sampled in. Data described herein is available at http://www.igs.cnrs-mrs.fr/Tara_Agulhas, at EBI under the project identifiers PRJEB402 and
PRJEB7988 and at PANGAEA (57-59). The data release policy regarding future public release of Tara Oceans data is described in Pesant *et al.* (50). All authors approved the final manuscript. This article is contribution number ZZZ of Tara Oceans. Supplement contains additional data.

***Tara* Oceans coordinators:**
Silvia G. Acinas[1], Peer Bork[2], Emmanuel Boss[3], Chris Bowler[4], Colomban de Vargas[5,6], Michael Follows[7], Gabriel Gorsky[8,9], Nigel Grimsley[10,11], Pascal Hingamp[12], Daniele Iudicone[13], Olivier Jaillon[14,15,16], Stefanie Kandels-Lewis[2,17], Lee Karp-Boss[3], Eric Karsenti[4,17], Uros Krzic[18], Fabrice Not[5,6], Hiroyuki Ogata[19], Stephane Pesant[20,21], Jeroen Raes[22,23,24], Emmanuel G. Reynaud[25], Christian Sardet[26,27], Mike Sieracki[28], Sabrina Speich[29,30], Lars Stemmann[8], Matthew B. Sullivan[31], Shinichi Sunagawa[2], Didier Velayoudon[32], Jean Weissenbach[14,15,16], Patrick Wincker[14,15,16]

[1]Department of Marine Biology and Oceanography, Institute of Marine Science (ICM)-CSIC, Pg. Marítim de la Barceloneta, 37-49, Barcelona E08003, Spain.
[2]Structural and Computational Biology, European Molecular Biology Laboratory, Meyerhofstr. 1, 69117 Heidelberg, Germany.
[3]School of Marine Sciences, University of Maine, Orono, Maine, USA.
[4]Ecole Normale Supérieure, Institut de Biologie de l'ENS (IBENS), and Inserm U1024, and CNRS UMR 8197, Paris, F-75005 France.
[5]CNRS, UMR 7144, Station Biologique de Roscoff, Place Georges Teissier, 29680 Roscoff, France.
[6]Sorbonne Universités, UPMC Univ Paris 06, UMR 7144, Station Biologique de Roscoff, Place Georges Teissier, 29680 Roscoff, France.
[7]Dept of Earth, Atmospheric and Planetary Sciences, Massachusetts Institute of Technology, Cambridge, USA.
[8]CNRS, UMR 7093, LOV, Observatoire Océanologique, F-06230, Villefranche-sur-mer, France.
[9]Sorbonne Universités, UPMC Univ Paris 06, UMR 7093, LOV, Observatoire Océanologique, F-06230, Villefranche-sur-mer, France.
[10]CNRS UMR 7232, BIOM, Avenue du Fontaulé, 66650 Banyuls-sur-Mer, France.
[11]Sorbonne Universités Paris 06, OOB UPMC, Avenue du Fontaulé, 66650 Banyuls-sur-Mer France.
[12]Aix Marseille Université CNRS IGS UMR 7256 13288 Marseille France.
[13]Stazione Zoologica Anton Dohrn, Villa Comunale, 80121, Naples, Italy.
[14]CEA - Institut de Génomique, GENOSCOPE, 2 rue Gaston Crémieux, 91057 Evry, France.
[15]CNRS, UMR 8030, CP5706, Evry France.
[16]Université d'Evry, UMR 8030, CP5706, Evry France.

[17]Directors' Research, European Molecular Biology Laboratory, Heidelberg, Germany.
[18]Cell Biology and Biophysics, European Molecular Biology Laboratory, Meyerhofstr. 1, 69117 Heidelberg, Germany.
[19]Institute for Chemical Research, Kyoto University, Gokasho, Uji, Kyoto, 611-001, Japan.
[20]PANGAEA, Data Publisher for Earth and Environmental Science, University of Bremen, Bremen, Germany.
[21]MARUM, Center for Marine Environmental Sciences, University of Bremen, Bremen, Germany.
[22]Department of Microbiology and Immunology, Rega Institute, KU Leuven, Herestraat 49, 3000 Leuven, Belgium.
[23]Center for the Biology of Disease, VIB, Herestraat 49, 3000 Leuven, Belgium.
[24]Department of Applied Biological Sciences, Vrije Universiteit Brussel, Pleinlaan 2, 1050 Brussels, Belgium.
[25]Earth Institute, University College Dublin, Dublin, Ireland.
[26]CNRS, UMR 7009 Biodev, Observatoire Océanologique, F-06230 Villefranche-sur-mer, France.
[27]Sorbonne Universités, UPMC Univ Paris 06, UMR 7009 Biodev, F-06230 Observatoire Océanologique, Villefranche-sur-mer, France.
[28]Bigelow Laboratory for Ocean Sciences, East Boothbay, USA.
[29]Department of Geosciences, Laboratoire de Météorologie Dynamique (LMD), Ecole Normale Supérieure, 24 rue Lhomond 75231 Paris Cedex 05 France.
[30]Laboratoire de Physique des Océan UBO-IUEM Palce Copernic 29820 Polouzané, France.
[31]Department of Ecology and Evolutionary Biology, University of Arizona, 1007 E Lowell Street, Tucson, AZ, 85721, USA.
[32]DVIP Consulting, Sèvres, France.

Fig. 1: The oceanic circulation around the Agulhas choke point and location of Tara Oceans stations.

The map shows the location of sampling stations, together with trajectories of the young and old Agulhas rings (TARA_068 & TARA_078, red and green tracks, respectively). The stations here considered as representative of the main basins are: 1) TARA_052, TARA_064, and TARA_065 for Indian Ocean (IO); 2) TARA_070, TARA_072 and TARA_076 for the South Atlantic Ocean (SAO) and 3) TARA_082, TARA_084 and TARA_085 for the Southern Ocean (SO). The mean ocean circulation is schematized by arrows (currents) and background colors (surface climatological dynamic height (0/2,000 dbar from CARS2009; www.cmar.csiro.au/cars, 61). Agulhas rings are depicted as circles. The Antarctic Circumpolar Current front positions are from (13).

Fig. 2: Agulhas system plankton community structure

A/ Plankton community structure of the Indian Ocean, South Atlantic Ocean, Southern Ocean and Agulhas rings. Bacterial 0.2-3 µm assemblage structure was determined by counting clade-specific marker-genes from bacterial metagenomes. Size fractionated (0.8-5, 20-180, 180-2 000 µm) eukaryotic assemblage structure was determined using V9 rDNA barcodes. Nucleo-Cytoplasmic Large DNA Viruses (NCLDV) 0.2-3 µm assemblage structure was determined by phylogenetic mapping using sixteen NCLDV marker genes. OTU abundances were converted to presence/absence to hierarchically cluster samples using Jaccard distance. B/ Network of pairwise comparisons of shared V9 rDNA barcode richness (shared barcode richness) between the 11 sampling stations of the study. The width of each edge is proportional to the number of shared barcodes between corresponding sampling stations. C/ Boxplot of shared barcode richness between stations for 0.8-5, 20-180 and 180-2 000 µm size fractions. The shared barcode richness analysis considers that two V9 rDNA barcodes are shared between two samples if they are 100% identical over their whole length. Shared barcode richness between two samples s1 & s2 is expressed as the proportion of shared barcode richness relative to the average internal barcode richness of samples s1 & s2. IO: Indian Ocean; SAO: South Atlantic Ocean, SO: Southern Ocean, Y.RING: Young Ring; O.RING: Old Ring.

Fig. 3: Diversity of plankton population specific to Indian and Atlantic Oceans

A/ Boxplot of 16S (0.2-3 μm) and V9 rDNA barcodes richness (0.8-5, 20-180 and 180-2000 μm size fractions). Each box represents 3 sampling stations combined into Indian, South Atlantic and Southern Ocean. Single Agulhas ring stations are represented as red (young ring) and orange (old ring) crosses. B/ Plankton sub-OTU richness filtering across the Agulhas choke point. Each vertical bar represents a single eukaryotic plankton OTU, each of which contains >10 distinct V9 rDNA barcodes (14). For each OTU are represented the number of distinct barcodes (sub-OTU richness) found exclusively in the South Atlantic Ocean (blue), exclusively in the Indian Ocean (pink), and in both South Atlantic Ocean and Indian Ocean (grey). OTUs are grouped by taxonomic annotation (indicated above the bar plot). For each taxonomic group, the percentage of OTUs with higher sub-OTU richness in the Indian Ocean (shaded in pink) or in the South Atlantic Ocean (shaded in blue) are indicated, respectively at the top and bottom of the bar plot. A total of 1307 OTUs are presented, representing 98% of total V9 rDNA barcode abundance.

Fig. 4: Properties of the young Agulhas ring (TARA_068).
A/ Daily sea surface height around young Agulhas ring station TARA_068 (DT Absolute Dynamic Topography (ADT) from http://www.aviso.altimetry.fr/). R, C1 and C2 respectively denote the centers of the Agulhas ring and two cyclonic eddies. The contour interval is 0.02 dyn.m. The ADT values are for September 13th, 2010. Light grey isolines: ADT < 0.46 dyn. m. The crosses indicate the CTD stations while the square symbol indicates the position of the biological station TARA_068. The biological station coincides with the westernmost CTD station. ADT is affected by interpolation errors, which is why CTD casts were performed at sea to have a fine-scale description of the feature before defining the position of the biological station (23). Superimposed are the continuous underway temperatures (°C) from the on-board thermosalinograph. B/ Same as panel A but at the regional scale. Round symbols correspond to biological sampling stations. The contour interval is 0.1 dyn.m. C/ Seasonal distribution of the median values of the mixed layer depths and temperatures at 10m (from ARGO) provided by the IFREMER/LOS Mixed Layer Depth Climatology L2 database (www.ifremer.fr/cerweb/deboyer/mld) updated to July 27th 2011. The mixed layer is defined using a temperature criteria. The star symbol represents the young ring station TARA_068. Inset: geographic position of the areas used to select the mixed layer and temperature data. The mixed layer depth measured at TARA_068 is outside the 90th percentile of the distribution of mixed layer depths for the same month for both the subtropical (red and magenta) regions. The temperature matches the median for the same month and region of sampling. D/ Nitrites (NO2) concentrations in mmol/m3.

Fig. 5: Plankton diversity patterns.
A/ Schematic representation of the four scenarios (I-IV): plankton is transported from Indian (pink, right) to South Atlantic Oceans (blue, left) through the choke point (red, CP). The thickness of each colored section represents the level of diversity specific to each region. The observed percentage of V9 rDNA OTUs corresponding to each scenario is indicated in the pie charts to the left (out of 1063 OTUs of the full V9 rDNA barcode dataset). B/ V9 rDNA OTU diversity patterns for copepods and Bacillariophyta. Each circle on the charts represents a V9 rDNA OTU plotted with coordinates proportional to ribotypes specific to Indian Ocean (x-axis) and South Atlantic Ocean (y-axis). For instance, the copepod Acartia negligens in the top right corner of sector II corresponds to the “bow tie” scenario II of panel A (i.e. a copepod with representative V9 rDNA barcodes in both Indian and South Atlantic Oceans, the vast majority of

which are specific to their respective ocean basin). In contrast, the majority of barcodes for Siloncalanus sinensis in sector III are found in both Indian and South Atlantic Oceans (cosmopolitan OTU corresponding to the "Everything is everywhere" flat diversity diagram of panel A, scenario III). If more than 10 barcodes were found in the young Agulhas ring (TARA_068), their distribution is indicated in a pie chart (colors are coded in the legend inset), otherwise the OTU is represented by an empty circle. Circle sizes are proportional to the number of considered barcodes for each OTU. The Bacillariophyta OTU defined as 'Raphid pennate sp.' likely corresponds to the Pseudo-nitzschia cells observed by light microscopy.

Fig. 6: Modeled nitrogen stocks along Agulhas ring track
A/ Simulated primary production (PP) in the Agulhas system using the MIT-GCM model. The solid black line shows the average northwesterly path of 12 distinct virtual Agulhas rings tracked over the course of the simulation. Color scale for PP is given in the top right inset, with warmer colors indicating higher PP. B/ Modeled profiles of NO3, NO2 and NH4 along the Agulhas ring average track (x-axis) presented in A. The y-axis is the depth (in meters) in the water column. The color scale is given in the top right inset, with warmer colors indicating higher concentrations of nitrogen compounds.

Fig. 7: Nitrite anomaly in young Agulhas ring is accompanied by shifts in nitrogen pathway related genes
Metagenomic over- and under-represented nitrogen pathway genes in young Agulhas ring. Over- (red circles) and under- (green circles) represented metagenome functional annotations (KEGG Orthologs, KO#) involved in the nitrogen pathway in the young ring compared to Indian and South Atlantic Oceans reference stations, at surface and deep chlorophyll maximum depth. Pie charts inside circles represent the taxonomic distribution for each ortholog.

Fig. 8: Picocyanobacterial clade shift in the young Agulhas ring.
A/ Relative abundance of Prochlorococcus and Synechococcus clades estimated by petB read recruitments from 0.2-3 μm metagenomes. Solid squares correspond to read counts normalized based on the sequencing effort (right axis). B/ Relative abundance of nirA gene from Prochlorococcus and Synechococcus clades estimated by number of reads recruited from 0.2-3 μm metagenomes. The bar colors correspond to cyanobacterial clades indicated in the inset legends for each panel. Solid squares correspond to the number of reads recruited (right axis). Data is shown for stations 52 to 78 only as too few cyanobacteria were found in Southern Ocean stations TARA_082, TARA_84 and TARA_85.

Supplementary Materials:
Table S1: Sample information and accession numbers in the PANGAEA archive.

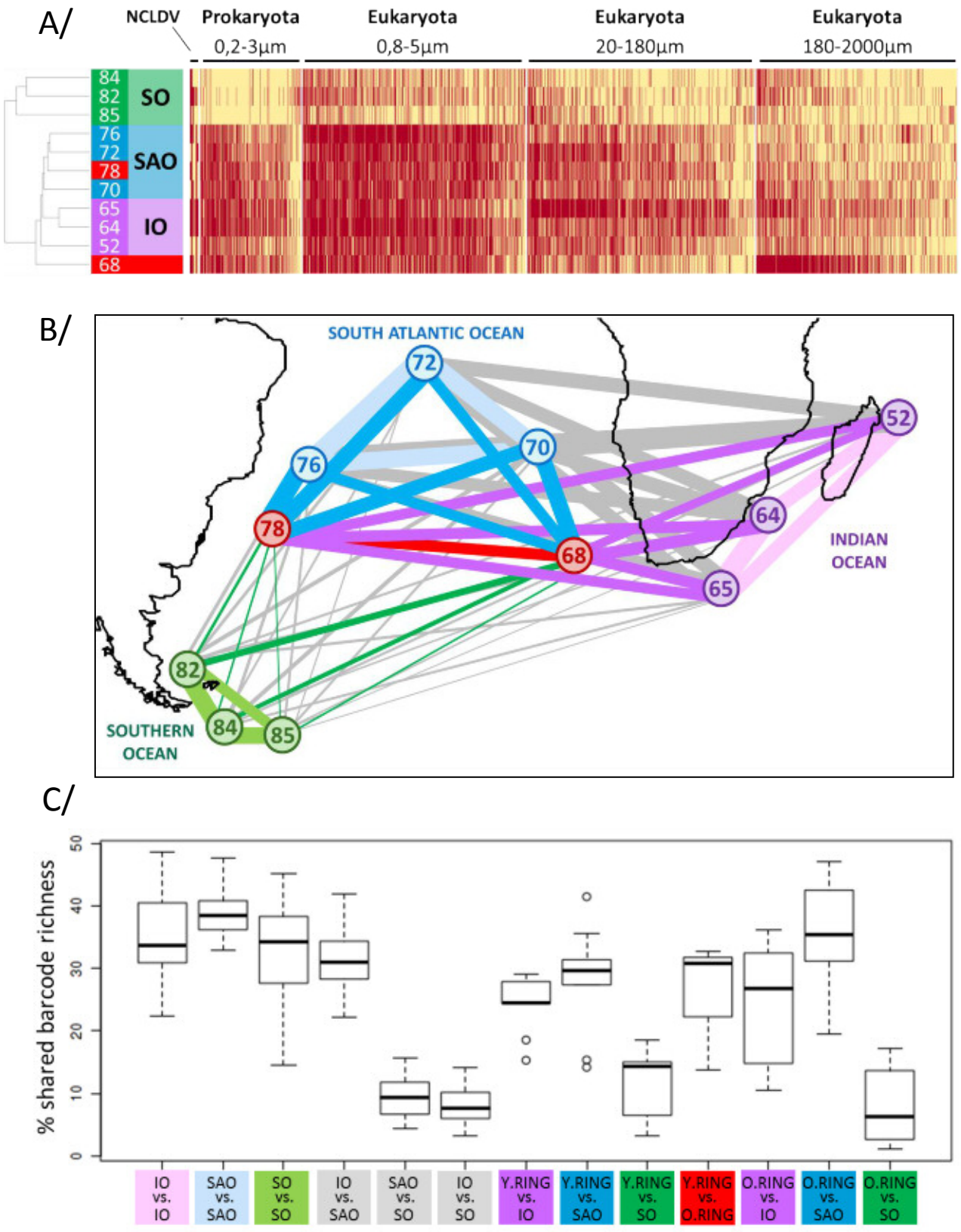
A/
NCLDV
Prokaryota
0,2-3µm
Eukaryota
0,8-5µm
Eukaryota
20-180µm
Eukaryota
180-2000µm
84
82
85
SO
76
72
78
70
SAO
65
64
52
68
IO
B/
SOUTH ATLANTIC OCEAN
72
76
70
52
78
64
68
INDIAN
OCEAN
65
82
SOUTHERN
OCEAN
84
85
C/
% shared barcode richness
0
10
20
30
40
50
IO vs. IO
SAO vs. SAO
SO vs. SO
IO vs. SAO
SAO vs. SO
IO vs. SO
Y.RING vs. IO
Y.RING vs. SAO
Y.RING vs. SO
Y.RING vs. O.RING
O.RING vs. IO
O.RING vs. SAO
O.RING vs. SO

A/

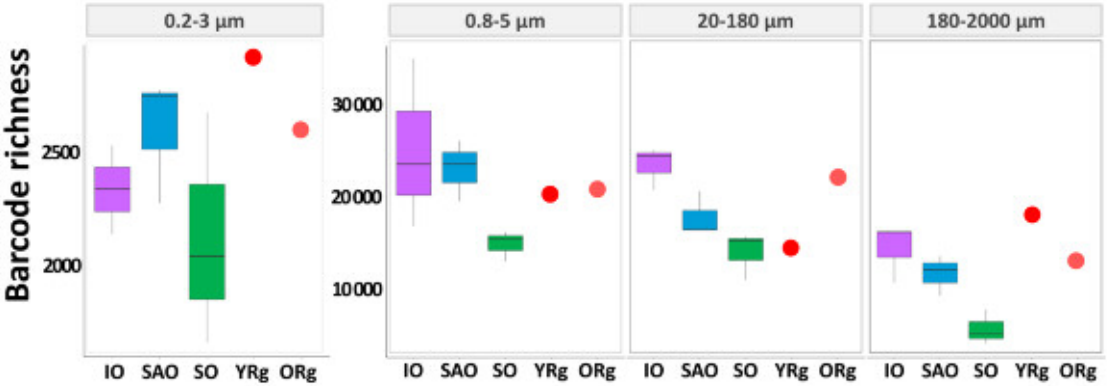
0.2-3 µm
0.8-5 µm
20-180 µm
180-2000 µm
Barcode richness
2500
2000
30000
20000
10000
IO SAO SO YRg ORg

B/

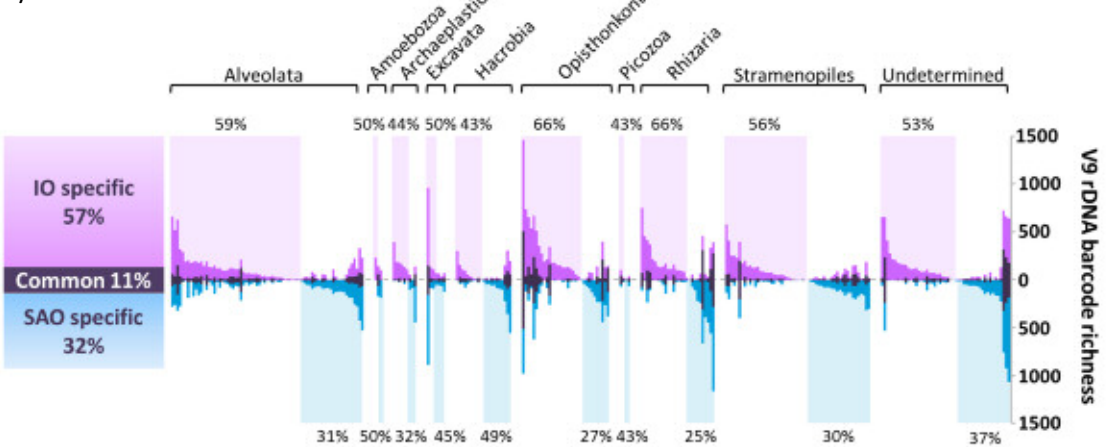
Alveolata
Amoebozoa
Archaeplastida
Excavata
Hacrobia
Opisthonkonta
Picozoa
Rhizaria
Stramenopiles
Undetermined
59% 50% 44% 50% 43% 66% 43% 66% 56% 53%
IO specific 57%
Common 11%
SAO specific 32%
31% 50% 32% 45% 49% 27% 43% 25% 30% 37%
1500 1000 500 0 500 1000 1500
V9 rDNA barcode richness

A/ Diversity scenarios

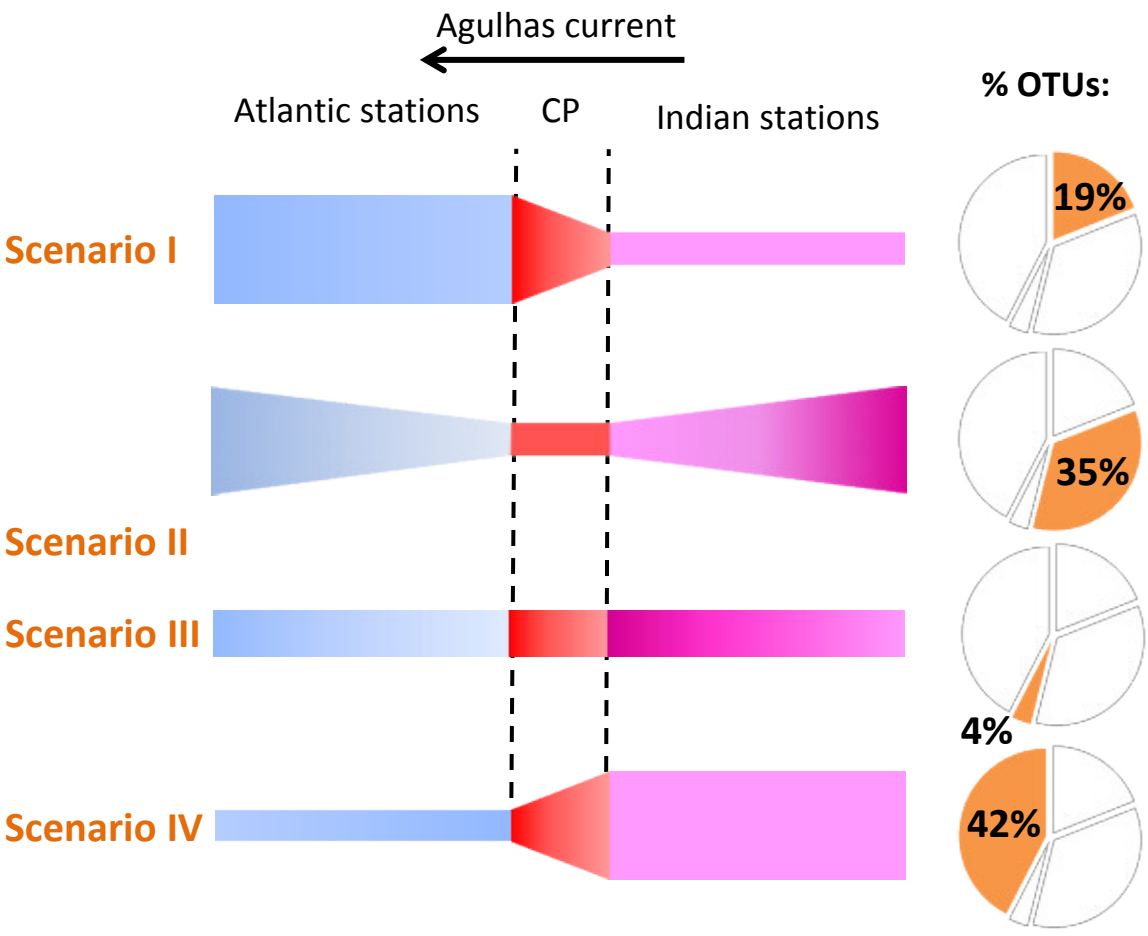

B/ Diversity patterns

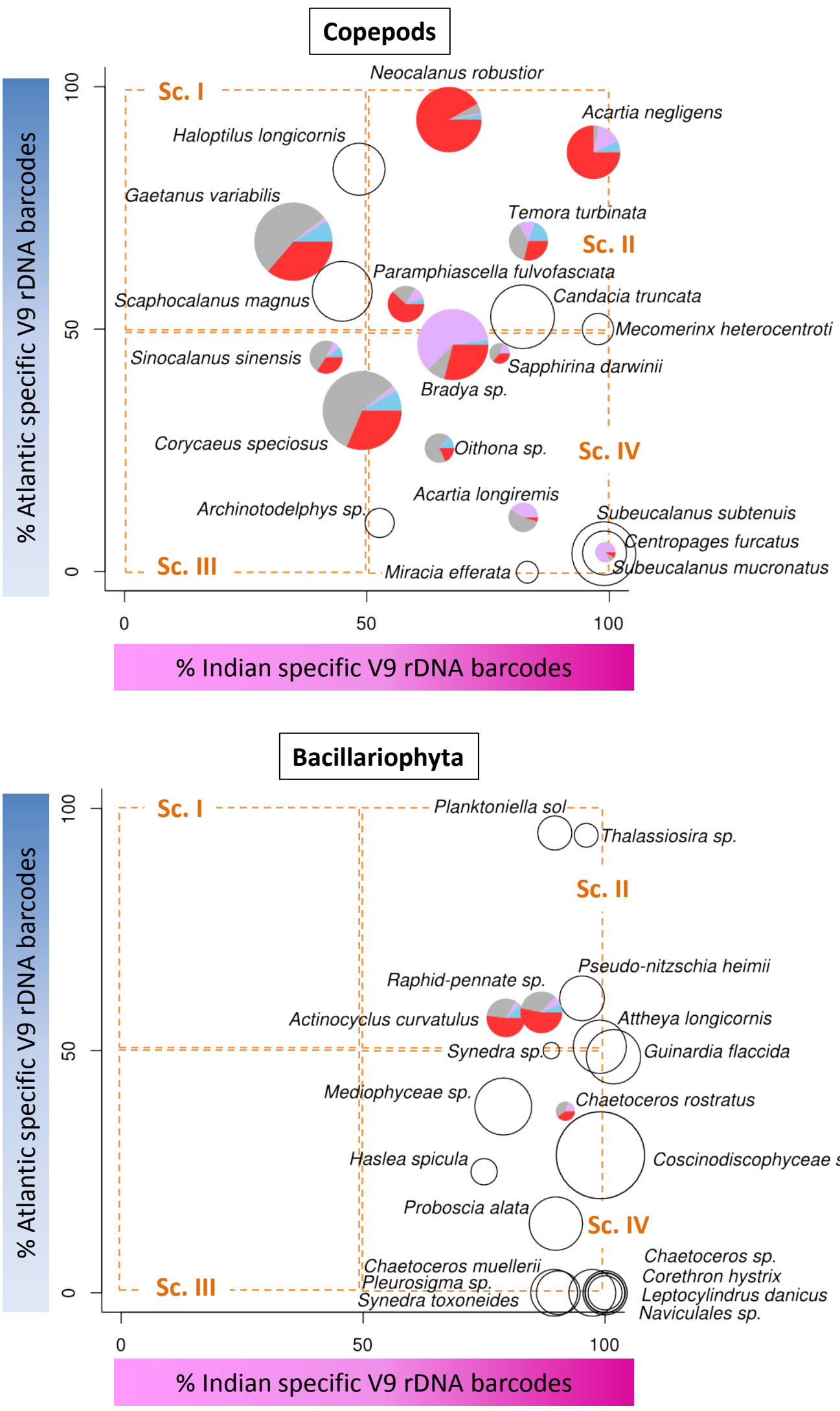

Ring barcodes:

- shared with Indian stations (YR-IO)
- shared with Atlantic stations (YR-SAO)
- shared with Indian and Atlantic stations (YR-IO-SAO)
- specific to the ring (YR)

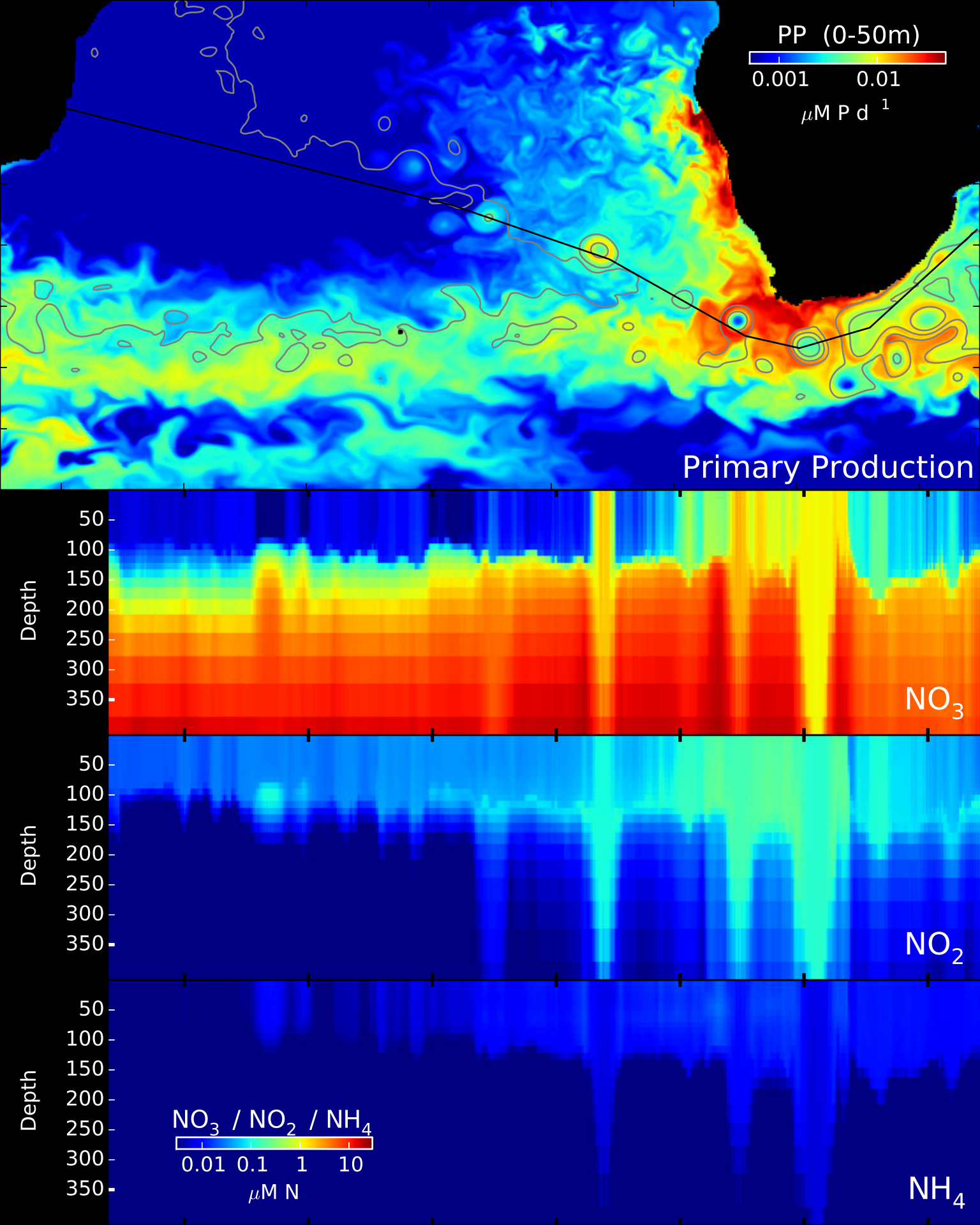
PP (0-50m)
0.001
0.01
μM P d 1
Primary Production
Depth
50
100
150
200
250
300
350
NO3
NO2
NH4
NO3 / NO2 / NH4
0.01 0.1 1 10
μM N

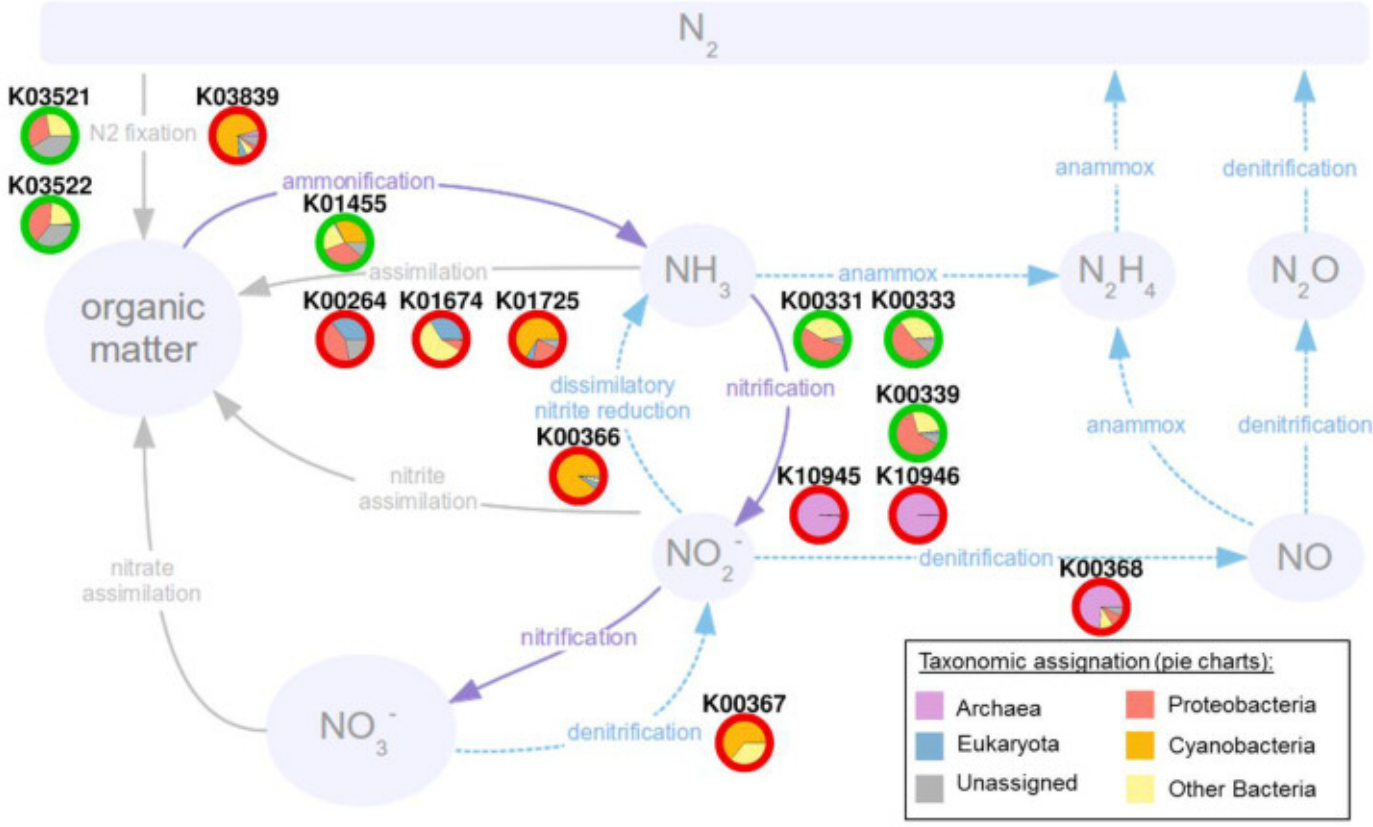
N_2
K03521
K03839
N2 fixation
K03522
ammonification
K01455
organic matter
assimilation
K00264
K01674
K01725
NH_3
anammox
N_2H_4
anammox
denitrification
N_2O
K00331
K00333
dissimilatory nitrite reduction
nitrification
K00339
K00366
anammox
denitrification
nitrite assimilation
K10945
K10946
NO_2^-
denitrification
NO
K00368
nitrate assimilation
nitrification
NO_3^-
denitrification
K00367
Taxonomic assignation (pie charts):
Archaea
Eukaryota
Unassigned
Proteobacteria
Cyanobacteria
Other Bacteria

A/ *petB* marker

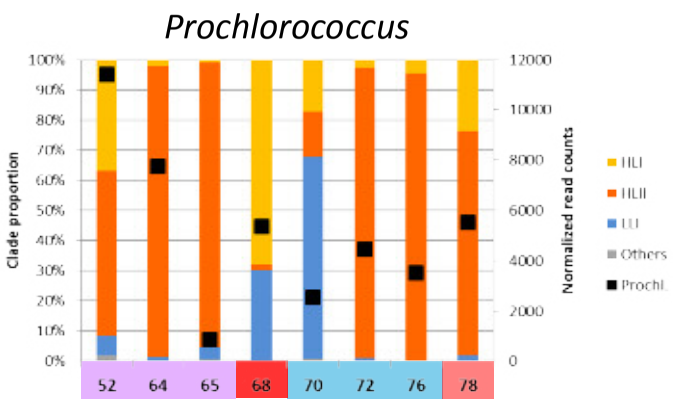

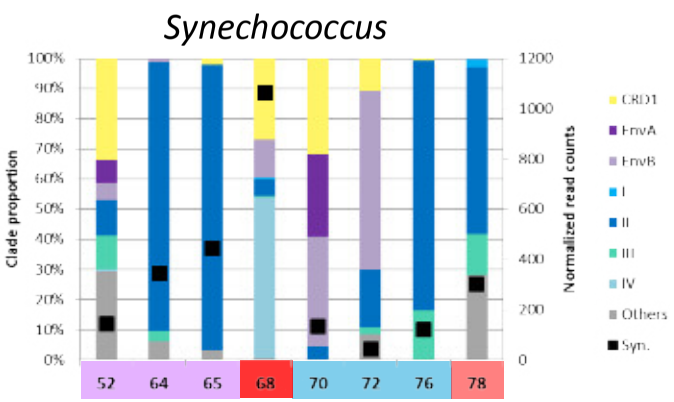

B/ *nirA* gene

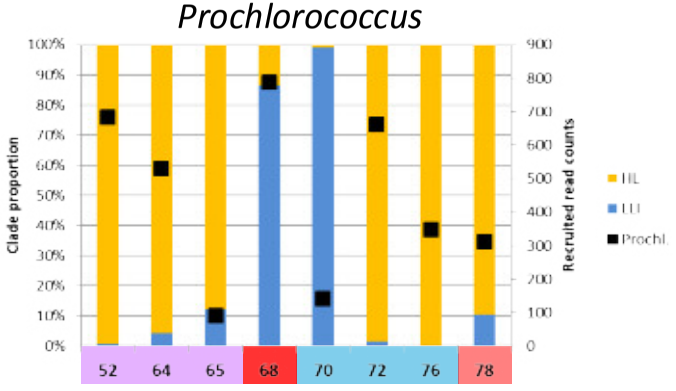

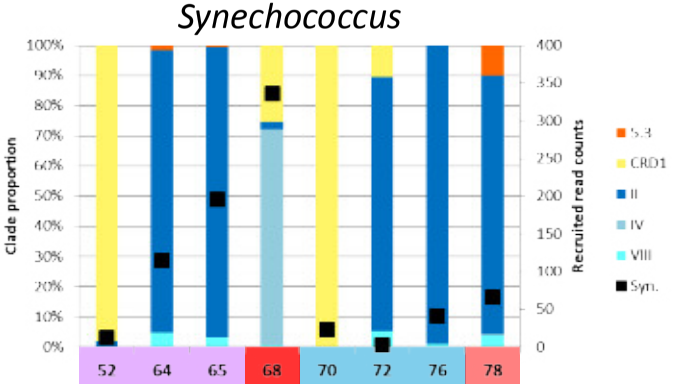

Table S1: Sample accession numbers in PANGAEA archive.

Sample label [TARA_station#_environmental-feature_size-fraction]	PANGAEA sample identifier	Corresponding contextual data published at PANGAEA	Station identifier [TARA_station#]	Date/Time [yyyy-mm-ddThh:mm]	Latitude [degrees North]	Longitude [degrees East]	Sampling depth [m]	Environmental Feature	Size fraction lower threshold [micrometre]	Size fraction upper threshold [micrometre]	Marine pelagic biomes (Longhurst 2007)	Ocean and sea regions (IHO General Sea Areas 1953) [MRGID registered at www.marineregions.com]	Marine pelagic biomes (Longhurst 2007) [MRGID registered at www.marineregions.com]
TARA_052_DCM_0.22-1.6	TARA_B1000002	ftp://www.pangaea.de/search?All&q=TARA_B1000002	TARA_052	2010-05-17T11:42	-16.9534	53.9601	75	(DCM) deep chlorophyll maximum layer (ENVO:01000326)	0.22	1.6	Trades Biome	(IO) Indian Ocean [MRGID:1904]	(ISSG) Indian South Subtropical Gyre Province [MRGID:21472]
TARA_052_SRF_0.22-1.6	TARA_B1000002	ftp://www.pangaea.de/search?All&q=TARA_B1000002	TARA_052	2010-05-17T04:10	-16.957	53.9801	5	(SRF) surface water layer (ENVO:00002042)	0.22	1.6	Trades Biome	(IO) Indian Ocean [MRGID:1904]	(ISSG) Indian South Subtropical Gyre Province [MRGID:21472]
TARA_052_SRF_0.8-5	TARA_N0000005 98	ftp://www.pangaea.de/search?All&q=TARA_N0000005	TARA_052	2010-05-17T04:10	-16.957	53.9801	5	(SRF) surface water layer (ENVO:00002042)	0.8	5	Trades Biome	(IO) Indian Ocean [MRGID:1904]	(ISSG) Indian South Subtropical Gyre Province [MRGID:21472]
TARA_052_SRF_20-180	TARA_N0000005 89	ftp://www.pangaea.de/search?All&q=TARA_N0000005	TARA_052	2010-05-17T06:48	-16.9672	53.9537	5	(SRF) surface water layer (ENVO:00002042)	20	180	Trades Biome	(IO) Indian Ocean [MRGID:1904]	(ISSG) Indian South Subtropical Gyre Province [MRGID:21472]
TARA_052_SRF_180-2000	TARA_N0000005 81	ftp://www.pangaea.de/search?All&q=TARA_N0000005	TARA_052	2010-05-17T04:10	-16.9567	53.9809	5	(SRF) surface water layer (ENVO:00002042)	180	2000	Trades Biome	(IO) Indian Ocean [MRGID:1904]	(ISSG) Indian South Subtropical Gyre Province [MRGID:21472]
TARA_064_DCM_0.22-3	TARA_B1000004	ftp://www.pangaea.de/search?All&q=TARA_B1000004	TARA_064	2010-07-08T06:21	-29.5333	37.9117	65	(DCM) deep chlorophyll maximum layer (ENVO:01000326)	0.22	3	Coastal Biome	(IO) Indian Ocean [MRGID:1904]	(EAFR) Eastern Africa Coastal Province [MRGID:21473]
TARA_064_SRF_0.22-3	TARA_B1000004	ftp://www.pangaea.de/search?All&q=TARA_B1000004	TARA_064	2010-07-07T04:48	-29.5019	37.9889	5	(SRF) surface water layer (ENVO:00002042)	0.22	3	Coastal Biome	(IO) Indian Ocean [MRGID:1904]	(EAFR) Eastern Africa Coastal Province [MRGID:21473]
TARA_064_SRF_0.8-5	TARA_N0000005 22	ftp://www.pangaea.de/search?All&q=TARA_N0000005	TARA_064	2010-07-07T04:48	-29.5019	37.9889	5	(SRF) surface water layer (ENVO:00002042)	0.8	5	Coastal Biome	(IO) Indian Ocean [MRGID:1904]	(EAFR) Eastern Africa Coastal Province [MRGID:21473]
TARA_064_SRF_20-180	TARA_N0000005 26	ftp://www.pangaea.de/search?All&q=TARA_N0000005	TARA_064	2010-07-07T07:53	-29.4985	37.9926	5	(SRF) surface water layer (ENVO:00002042)	20	180	Coastal Biome	(IO) Indian Ocean [MRGID:1904]	(EAFR) Eastern Africa Coastal Province [MRGID:21473]
TARA_064_SRF_180-2000	TARA_N0000005 39	ftp://www.pangaea.de/search?All&q=TARA_N0000005	TARA_064	2010-07-07T05:17	-29.5018	37.9887	5	(SRF) surface water layer (ENVO:00002042)	180	2000	Coastal Biome	(IO) Indian Ocean [MRGID:1904]	(EAFR) Eastern Africa Coastal Province [MRGID:21473]
TARA_065_DCM_0.22-3	TARA_B0000004	ftp://www.pangaea.de/search?All&q=TARA_B0000004	TARA_065	2010-07-12T11:03:2	-35.2421	26.3048	30	(DCM) deep chlorophyll maximum layer (ENVO:01000326)	0.22	3	Coastal Biome	(IO) Indian Ocean [MRGID:1904]	(EAFR) Eastern Africa Coastal Province [MRGID:21473]
TARA_065_SRF_0.22-3	TARA_B0000004	ftp://www.pangaea.de/search?All&q=TARA_B0000004	TARA_065	2010-07-12T05:59	-35.1728	26.2868	5	(SRF) surface water layer (ENVO:00002042)	0.22	3	Coastal Biome	(IO) Indian Ocean [MRGID:1904]	(EAFR) Eastern Africa Coastal Province [MRGID:21473]
TARA_065_SRF_0.8-5	TARA_N0000009 59	ftp://www.pangaea.de/search?All&q=TARA_N0000009	TARA_065	2010-07-12T05:59	-35.1728	26.2868	5	(SRF) surface water layer (ENVO:00002042)	0.8	5	Coastal Biome	(IO) Indian Ocean [MRGID:1904]	(EAFR) Eastern Africa Coastal Province [MRGID:21473]
TARA_065_SRF_20-180	TARA_N0000009 68	ftp://www.pangaea.de/search?All&q=TARA_N0000009	TARA_065	2010-07-12T10:30	-35.2351	26.3022	5	(SRF) surface water layer (ENVO:00002042)	20	180	Coastal Biome	(IO) Indian Ocean [MRGID:1904]	(EAFR) Eastern Africa Coastal Province [MRGID:21473]
TARA_065_SRF_180-2000	TARA_N0000009 81	ftp://www.pangaea.de/search?All&q=TARA_N0000009	TARA_065	2010-07-12T06:36	-35.1808	26.2879	5	(SRF) surface water layer (ENVO:00002042)	180	2000	Coastal Biome	(IO) Indian Ocean [MRGID:1904]	(EAFR) Eastern Africa Coastal Province [MRGID:21473]
TARA_068_DCM_0.22-3	TARA_B1000004	ftp://www.pangaea.de/search?All&q=TARA_B1000004	TARA_068	2010-09-14T13:30	-31.027	4.6802	50	(DCM) deep chlorophyll maximum layer (ENVO:01000326)	0.22	3	Trades Biome	(SAO) South Atlantic Ocean [MRGID:1914]	(SATL) South Atlantic Gyral Province [MRGID:21459]
TARA_068_SRF_0.22-3	TARA_B1000004	ftp://www.pangaea.de/search?All&q=TARA_B1000004	TARA_068	2010-09-14T06:55	-31.0266	4.665	5	(SRF) surface water layer (ENVO:00002042)	0.22	3	Trades Biome	(SAO) South Atlantic Ocean [MRGID:1914]	(SATL) South Atlantic Gyral Province [MRGID:21459]
TARA_068_SRF_0.8-5	TARA_N0000007 22	ftp://www.pangaea.de/search?All&q=TARA_N0000007	TARA_068	2010-09-14T06:55	-31.0266	4.665	5	(SRF) surface water layer (ENVO:00002042)	0.8	5	Trades Biome	(SAO) South Atlantic Ocean [MRGID:1914]	(SATL) South Atlantic Gyral Province [MRGID:21459]
TARA_068_SRF_20-180	TARA_N0000007 05	ftp://www.pangaea.de/search?All&q=TARA_N0000007	TARA_068	2010-09-13T21:35	-31.0551	4.668	5	(SRF) surface water layer (ENVO:00002042)	20	180	Trades Biome	(SAO) South Atlantic Ocean [MRGID:1914]	(SATL) South Atlantic Gyral Province [MRGID:21459]
TARA_068_SRF_180-2000	TARA_N0000007 09	ftp://www.pangaea.de/search?All&q=TARA_N0000007	TARA_068	2010-09-13T20:20	-31.0507	4.6603	5	(SRF) surface water layer (ENVO:00002042)	180	2000	Trades Biome	(SAO) South Atlantic Ocean [MRGID:1914]	(SATL) South Atlantic Gyral Province [MRGID:21459]
TARA_070_SRF_0.22-3	TARA_B1000004	ftp://www.pangaea.de/search?All&q=TARA_B1000004	TARA_070	2010-09-21T06:55	-20.4091	-3.1759	5	(SRF) surface water layer (ENVO:00002042)	0.22	3	Trades Biome	(SAO) South Atlantic Ocean [MRGID:1914]	(SATL) South Atlantic Gyral Province [MRGID:21459]
TARA_070_SRF_0.8-5	TARA_N0000006 78	ftp://www.pangaea.de/search?All&q=TARA_N0000006	TARA_070	2010-09-21T06:55	-20.4091	-3.1759	5	(SRF) surface water layer (ENVO:00002042)	0.8	5	Trades Biome	(SAO) South Atlantic Ocean [MRGID:1914]	(SATL) South Atlantic Gyral Province [MRGID:21459]
TARA_070_SRF_20-180	TARA_N0000006 62	ftp://www.pangaea.de/search?All&q=TARA_N0000006	TARA_070	2010-09-21T08:23	-20.3943	-3.2085	5	(SRF) surface water layer (ENVO:00002042)	20	180	Trades Biome	(SAO) South Atlantic Ocean [MRGID:1914]	(SATL) South Atlantic Gyral Province [MRGID:21459]
TARA_070_SRF_180-2000	TARA_N0000006 66	ftp://www.pangaea.de/search?All&q=TARA_N0000006	TARA_070	2010-09-21T07:22	-20.4035	-3.1859	5	(SRF) surface water layer (ENVO:00002042)	180	2000	Trades Biome	(SAO) South Atlantic Ocean [MRGID:1914]	(SATL) South Atlantic Gyral Province [MRGID:21459]
TARA_072_DCM_0.22-3	TARA_B1000004	ftp://www.pangaea.de/search?All&q=TARA_B1000004	TARA_072	2010-10-05T15:35	-8.7296	-17.9604	100	(DCM) deep chlorophyll maximum layer (ENVO:01000326)	0.22	3	Trades Biome	(SAO) South Atlantic Ocean [MRGID:1914]	(SATL) South Atlantic Gyral Province [MRGID:21459]
TARA_072_SRF_0.22-3	TARA_B1000004	ftp://www.pangaea.de/search?All&q=TARA_B1000004	TARA_072	2010-10-05T08:00	-8.7789	-17.9099	5	(SRF) surface water layer (ENVO:00002042)	0.22	3	Trades Biome	(SAO) South Atlantic Ocean [MRGID:1914]	(SATL) South Atlantic Gyral Province [MRGID:21459]
TARA_072_SRF_0.8-5	TARA_N0000008 31	ftp://www.pangaea.de/search?All&q=TARA_N0000008	TARA_072	2010-10-05T08:00	-8.7789	-17.9099	5	(SRF) surface water layer (ENVO:00002042)	0.8	5	Trades Biome	(SAO) South Atlantic Ocean [MRGID:1914]	(SATL) South Atlantic Gyral Province [MRGID:21459]
TARA_072_SRF_20-180	TARA_N0000008 39	ftp://www.pangaea.de/search?All&q=TARA_N0000008	TARA_072	2010-10-05T09:48	-8.7484	-17.9179	5	(SRF) surface water layer (ENVO:00002042)	20	180	Trades Biome	(SAO) South Atlantic Ocean [MRGID:1914]	(SATL) South Atlantic Gyral Province [MRGID:21459]
TARA_072_SRF_180-2000	TARA_N0000008 43	ftp://www.pangaea.de/search?All&q=TARA_N0000008	TARA_072	2010-10-05T08:20	-8.7726	-17.915	5	(SRF) surface water layer (ENVO:00002042)	180	2000	Trades Biome	(SAO) South Atlantic Ocean [MRGID:1914]	(SATL) South Atlantic Gyral Province [MRGID:21459]
TARA_076_DCM_0.22-3	TARA_B1000005	ftp://www.pangaea.de/search?All&q=TARA_B1000005	TARA_076	2010-10-16T16:58:3	-21.0292	-35.3498	150	(DCM) deep chlorophyll maximum layer (ENVO:01000326)	0.22	3	Trades Biome	(SAO) South Atlantic Ocean [MRGID:1914]	(SATL) South Atlantic Gyral Province [MRGID:21459]
TARA_076_SRF_0.22-3	TARA_B1000005	ftp://www.pangaea.de/search?All&q=TARA_B1000005	TARA_076	2010-10-16T09:55	-20.9354	-35.1803	5	(SRF) surface water layer (ENVO:00002042)	0.22	3	Trades Biome	(SAO) South Atlantic Ocean [MRGID:1914]	(SATL) South Atlantic Gyral Province [MRGID:21459]
TARA_076_SRF_0.8-5	TARA_N0000008 55	ftp://www.pangaea.de/search?All&q=TARA_N0000008	TARA_076	2010-10-16T09:55	-20.9354	-35.1803	5	(SRF) surface water layer (ENVO:00002042)	0.8	5	Trades Biome	(SAO) South Atlantic Ocean [MRGID:1914]	(SATL) South Atlantic Gyral Province [MRGID:21459]
TARA_076_SRF_20-180	TARA_N0000008 71	ftp://www.pangaea.de/search?All&q=TARA_N0000008	TARA_076	2010-10-16T11:18	-20.9514	-35.2273	5	(SRF) surface water layer (ENVO:00002042)	20	180	Trades Biome	(SAO) South Atlantic Ocean [MRGID:1914]	(SATL) South Atlantic Gyral Province [MRGID:21459]
TARA_076_SRF_180-2000	TARA_N0000008 79	ftp://www.pangaea.de/search?All&q=TARA_N0000008	TARA_076	2010-10-16T10:16	-20.9406	-35.196	5	(SRF) surface water layer (ENVO:00002042)	180	2000	Trades Biome	(SAO) South Atlantic Ocean [MRGID:1914]	(SATL) South Atlantic Gyral Province [MRGID:21459]
TARA_078_DCM_0.22-3	TARA_B1000005	ftp://www.pangaea.de/search?All&q=TARA_B1000005	TARA_078	2010-11-04T18:16:5	-30.1484	-43.2705	120	(DCM) deep chlorophyll maximum layer (ENVO:01000326)	0.22	3	Trades Biome	(SAO) South Atlantic Ocean [MRGID:1914]	(SATL) South Atlantic Gyral Province [MRGID:21459]
TARA_078_SRF_0.22-3	TARA_B1000005	ftp://www.pangaea.de/search?All&q=TARA_B1000005	TARA_078	2010-11-04T10:04	-30.1367	-43.2899	5	(SRF) surface water layer (ENVO:00002042)	0.22	3	Trades Biome	(SAO) South Atlantic Ocean [MRGID:1914]	(SATL) South Atlantic Gyral Province [MRGID:21459]
TARA_078_SRF_0.8-5	TARA_N0000006 20	ftp://www.pangaea.de/search?All&q=TARA_N0000006	TARA_078	2010-11-04T10:04	-30.1367	-43.2899	5	(SRF) surface water layer (ENVO:00002042)	0.8	5	Trades Biome	(SAO) South Atlantic Ocean [MRGID:1914]	(SATL) South Atlantic Gyral Province [MRGID:21459]
TARA_078_SRF_20-180	TARA_N0000015 10	ftp://www.pangaea.de/search?All&q=TARA_N0000015	TARA_078	2010-11-04T13:22	-30.1872	-43.2834	5	(SRF) surface water layer (ENVO:00002042)	20	180	Trades Biome	(SAO) South Atlantic Ocean [MRGID:1914]	(SATL) South Atlantic Gyral Province [MRGID:21459]
TARA_078_SRF_180-2000	TARA_N0000015 14	ftp://www.pangaea.de/search?All&q=TARA_N0000015	TARA_078	2010-11-04T11:31	-30.1506	-43.2877	5	(SRF) surface water layer (ENVO:00002042)	180	2000	Trades Biome	(SAO) South Atlantic Ocean [MRGID:1914]	(SATL) South Atlantic Gyral Province [MRGID:21459]
TARA_082_DCM_0.22-3	TARA_B1000007	ftp://www.pangaea.de/search?All&q=TARA_B1000007	TARA_082	2010-12-06T18:58	-47.2007	-57.9446	40	(DCM) deep chlorophyll maximum layer (ENVO:01000326)	0.22	3	Coastal Biome	(SAO) South Atlantic Ocean [MRGID:1914]	(FKLD) Southwest Atlantic Shelves Province [MRGID:21469]
TARA_082_SRF_0.22-3	TARA_B1000007	ftp://www.pangaea.de/search?All&q=TARA_B1000007	TARA_082	2010-12-06T10:33	-47.1863	-58.2902	5	(SRF) surface water layer (ENVO:00002042)	0.22	3	Coastal Biome	(SAO) South Atlantic Ocean [MRGID:1914]	(FKLD) Southwest Atlantic Shelves Province [MRGID:21469]
TARA_082_SRF_0.8-5	TARA_N0000013 86	ftp://www.pangaea.de/search?All&q=TARA_N0000013	TARA_082	2010-12-06T10:33	-47.1863	-58.2902	5	(SRF) surface water layer (ENVO:00002042)	0.8	5	Coastal Biome	(SAO) South Atlantic Ocean [MRGID:1914]	(FKLD) Southwest Atlantic Shelves Province [MRGID:21469]
TARA_082_SRF_20-180	TARA_N0000013 94	ftp://www.pangaea.de/search?All&q=TARA_N0000013	TARA_082	2010-12-06T12:32	-47.1966	-58.2349	5	(SRF) surface water layer (ENVO:00002042)	20	180	Coastal Biome	(SAO) South Atlantic Ocean [MRGID:1914]	(FKLD) Southwest Atlantic Shelves Province [MRGID:21469]
TARA_082_SRF_180-2000	TARA_N0000013 98	ftp://www.pangaea.de/search?All&q=TARA_N0000013	TARA_082	2010-12-06T11:34	-47.1899	-58.2724	5	(SRF) surface water layer (ENVO:00002042)	180	2000	Coastal Biome	(SAO) South Atlantic Ocean [MRGID:1914]	(FKLD) Southwest Atlantic Shelves Province [MRGID:21469]
TARA_084_SRF_0.22-3	TARA_B1000007	ftp://www.pangaea.de/search?All&q=TARA_B1000007	TARA_084	2011-01-03T11:05	-60.2287	-60.6476	5	(SRF) surface water layer (ENVO:00002042)	0.22	3	Polar Biome	(SO) Southern Ocean [MRGID:1907]	(ANTA) Antarctic Province [MRGID:21502]
TARA_084_SRF_0.8-5	TARA_N0000014 38	ftp://www.pangaea.de/search?All&q=TARA_N0000014	TARA_084	2011-01-03T11:05	-60.2287	-60.6476	5	(SRF) surface water layer (ENVO:00002042)	0.8	5	Polar Biome	(SO) Southern Ocean [MRGID:1907]	(ANTA) Antarctic Province [MRGID:21502]
TARA_084_SRF_20-180	TARA_N0000014 42	ftp://www.pangaea.de/search?All&q=TARA_N0000014	TARA_084	2011-01-03T13:58	-60.3046	-60.5715	5	(SRF) surface water layer (ENVO:00002042)	20	180	Polar Biome	(SO) Southern Ocean [MRGID:1907]	(ANTA) Antarctic Province [MRGID:21502]
TARA_084_SRF_180-2000	TARA_N0000013 62	ftp://www.pangaea.de/search?All&q=TARA_N0000013	TARA_084	2011-01-03T12:17	-60.2584	-60.6226	5	(SRF) surface water layer (ENVO:00002042)	180	2000	Polar Biome	(SO) Southern Ocean [MRGID:1907]	(ANTA) Antarctic Province [MRGID:21502]
TARA_085_DCM_0.22-3	TARA_B1000007	ftp://www.pangaea.de/search?All&q=TARA_B1000007	TARA_085	2011-01-06T19:34:2	-62.2231	-49.2139	90	(DCM) deep chlorophyll maximum layer (ENVO:01000326)	0.22	3	Polar Biome	(SO) Southern Ocean [MRGID:1907]	(ANTA) Antarctic Province [MRGID:21502]
TARA_085_SRF_0.22-3	TARA_B1000007	ftp://www.pangaea.de/search?All&q=TARA_B1000007	TARA_085	2011-01-06T10:38	-62.0385	-49.529	5	(SRF) surface water layer (ENVO:00002042)	0.22	3	Polar Biome	(SO) Southern Ocean [MRGID:1907]	(ANTA) Antarctic Province [MRGID:21502]
TARA_085_SRF_0.8-5	TARA_N0000010 28	ftp://www.pangaea.de/search?All&q=TARA_N0000010	TARA_085	2011-01-06T10:38	-62.0385	-49.529	5	(SRF) surface water layer (ENVO:00002042)	0.8	5	Polar Biome	(SO) Southern Ocean [MRGID:1907]	(ANTA) Antarctic Province [MRGID:21502]
TARA_085_SRF_20-180	TARA_N0000010 36	ftp://www.pangaea.de/search?All&q=TARA_N0000010	TARA_085	2011-01-06T15:29	-62.14	-49.3273	5	(SRF) surface water layer (ENVO:00002042)	20	180	Polar Biome	(SO) Southern Ocean [MRGID:1907]	(ANTA) Antarctic Province [MRGID:21502]
TARA_085_SRF_180-2000	TARA_N0000010 40	ftp://www.pangaea.de/search?All&q=TARA_N0000010	TARA_085	2011-01-06T12:45	-62.0773	-49.4534	5	(SRF) surface water layer (ENVO:00002042)	180	2000	Polar Biome	(SO) Southern Ocean [MRGID:1907]	(ANTA) Antarctic Province [MRGID:21502]